


Hydrodynamic magnetotransport in two-dimensional electron systems with macroscopic obstaclesP. S. Alekseev * and A. P. Dmitriev*Ioffe Institute, Politekhnicheskaya 26, Saint Petersburg 194021, Russia*

(Received 18 August 2023; revised 17 October 2023; accepted 18 October 2023; published 13 November 2023)

In high-quality conductors, the hydrodynamic regime of electron transport has recently been realized. In this paper, we theoretically investigate magnetotransport of a viscous electron fluid in samples with electron-impermeable obstacles. We use two approaches to describe the fluid flow. The first one is based on the equations of hydrodynamics of a charged fluid, which assume that the kinetic equation considers the two harmonics of the electron distribution function. The second approach is based on the equations that are obtained by considering three harmonics of the distribution function (quasihydrodynamics). Within the hydrodynamic approach, we consider the cases of the rough and smooth edges of disks, on which the electron scattering is diffusive or specular, respectively. The longitudinal magnetoresistivity turns out to be strong and negative, the same for both the rough and smooth disk edges up to small corrections. For rough disks, the Hall resistivity is equal to its standard value. For smooth disks, the Hall resistance acquires a small correction to the standard value, proportional to the Hall viscosity. In the quasihydrodynamic approach, we consider the case of smooth disks and small magnetic fields. In the regime when the flow is substantially different from the hydrodynamic one, the longitudinal resistivity does not depend on the shear stress relaxation time (but depends on the relaxation time of the third angular harmonic), while the correction to the standard Hall resistivity does not depend on both the relaxation times. We compare the results of the hydrodynamic calculation of the longitudinal resistance with the experimental data on magnetotransport in high-quality GaAs quantum wells with macroscopic defects. Agreement between theory and experiment evidences in favor of the realization of the hydrodynamic transport regime in such systems.

DOI: [10.1103/PhysRevB.108.205413](https://doi.org/10.1103/PhysRevB.108.205413)**I. INTRODUCTION****A. Hydrodynamics of viscous electron fluid in solids**

Frequent electron-electron collisions in high-quality conductors can lead to formation of a viscous electron fluid and realization of the hydrodynamic regime of charge transport [1]. In such systems, flows of the electron fluid are space inhomogeneous and determined by the geometry of a sample. This transport regime was recently reported for high-quality graphene [2–6], layered metal PdCoO₂ [7], Weyl semimetal WP₂ [8], and GaAs quantum wells [9–24]. Formation of the electron fluid was detected by a specific dependence of the resistance on the sample width [7,24], by observation of the negative nonlocal resistance [2,3,15,22], by the giant negative magnetoresistance [8–14,16,17,23,24], and by the magnetic resonance at the double cyclotron frequency [18–21,24].

There are various types of samples, being different in their geometry, where the viscous flows of the electron fluid were reported. The simplest one is the flat geometry of the Poiseuille flow in a long narrow sample. Such samples were studied in Refs. [2–8,24]. In this case, the flow is quasi-one-dimensional: Its profile depends only on the coordinate perpendicular to the longitudinal edges of the sample. Hydrodynamic flow of another type is formed in a high-quality

sample with localized macroscopic defects, on average homogeneously distributed and impermeable to electrons. In addition to this, the hydrodynamic electric transport has been studied in samples with a variety of complex geometries and complex arrangements of the electric contacts. For example, in Refs. [25,26], experimental and theoretical studies of the flow of the electron fluid in a long sample with one obstacle inside the bulk of the sample were performed.

Samples with macroscopic defects were experimentally studied in Refs. [13,27]. In Ref. [13], GaAs quantum well samples with oval defects, which appeared in the growth process, were examined. The electron mean free path related to scattering on these defects was determined from the sample resistance in zero magnetic field. In classically strong magnetic fields, the giant negative magnetoresistance, which evidences the formation of the viscous electron fluid [17], was observed in Ref. [13]. In Ref. [27], a set of samples of GaAs quantum wells was fabricated in which localized macroscopic obstacles of different densities were made using electron beam lithography and subsequent reactive ion etching. Extensive magnetotransport measurements of those samples were performed, in which various types of giant negative magnetoresistance were observed.

A first theory of the hydrodynamic charge transport of the two-dimensional (2D) electron fluid in a sample with localized defects was developed in Ref. [28]. Recently, in Ref. [29], a theory describing the crossover between the ohmic and the hydrodynamic regimes in such systems with increase of the

*alekseev_p_s@mail.ru

interparticle scattering rate was constructed. In Refs. [28,29] and other previous works, only electron fluid flows in the absence of magnetic fields were studied.

B. Flows of ordinary viscous fluids via porous media

In fact, the flows of uncharged fluids through an array of obstacles were systematically studied in ordinary hydrodynamics many years ago. The simplest example of such systems is a flow of water through an array of rocks in a mountain river. A more general example is the flow of a fluid via a porous media formed by randomly placed obstacles with various densities. An example of such systems in chemistry is the so-called *packed bed*, which is used to improve contact between two phases, a solid and liquid, in a chemical process.

The simplest qualitative description of such a system is the Kozeny-Carman equation [30,31]. It models the fluid flow in a sample of porous media as laminar fluid flow in a collection of curving passages crossing the packed bed. For each passage, the Poiseuille law was used to describe the laminar fluid flow in each section of the passage. Then the averaging of these results was performed to calculate the whole flow and the pressure drop in a sample.

There are two more rigorous analytical approaches for the calculation of the relation between the pressure drop and the magnitude of the flow in systems where the average distance between obstacles far exceeds their size.

The first one, known as the Brinkman approach, is the effective media approximation. In it, only the flow near one (any) obstacle is explicitly considered, while the influence of other obstacles is considered by introducing the term $-\mathbf{V}(\mathbf{r})/\tau$ into the Navier-Stokes equation [32]. Herewith, at a large distance from the considered obstacle, the hydrodynamic velocity $\mathbf{V}(\mathbf{r})$ is considered fixed and equal to the average flow velocity in the sample. Thus, the problem of the flow via an array of obstacles is reduced to the problem of a flow around a single obstacle immersed in a dissipative medium, the parameters of which are calculated in a self-consistent way. The microscopic derivation of the Brinkman equation and its corrections were described in Refs. [33,34].

The second approach is the so-called *cell model*. In it, the hydrodynamic Stokes problem was solved for a cell with one obstacle with boundary conditions on the obstacle boundary and on an imaginary cell boundary. Boundary conditions on the obstacle edges can be of two types: the Kuwabara conditions for sticky disks [35] and the Happel condition for mirror-edge disks [36,37]. The Happel condition requires the tangential component of the stress tensor to vanish at the disk boundary, while the Kuwabara condition requires zeroing of the full hydrodynamic velocity. As for the cell boundary, it is assumed that the hydrodynamic velocity on it is equal to the average velocity in the sample.

There is also a combined approach [38]: A boundary condition on an imaginary cell boundary matches the solution of the Stokes problem inside the cell (solution of usual Navier-Stokes equation) with the solution of the Brinkman problem with the Drude-like friction term $-\mathbf{V}(\mathbf{r})/\tau$ around the cell. The continuity of the velocity, pressure, and stress tensor at the cell boundary is required.

Further development of theory led to many quantitative, detailed results. It became possible to obtain relationships between the parameters of the effective media and of the flow properties to explain specific experimental data (see, for example, Refs. [39,40]).

In Ref. [17], a simple qualitative description has recently been proposed for the flow of a viscous 2D electron fluid in the magnetic field in a sample with macroscopic obstacles. An estimate for the sample resistance was derived for the case when the size of the obstacles is of the same order of magnitude as the distances between them. Consideration was performed by a method analogous to the simplest Kozeny-Carman method of description of flows an uncharged fluid via a porous media. The sample resistance turns out to be proportional to the diagonal viscosity, which leads to a strong negative magnetoresistance, like the one in a Poiseuille flow.

C. Hall effect in electron hydrodynamics

In studies of the hydrodynamic regime of electron transport, the Hall effect was of great interest. It was believed that the Hall voltage in such systems consists of two contributions: the main standard contribution, associated with the balance of the Lorentz force and the electric force, and a contribution arising due to the term of the off-diagonal Hall viscosity in the Navier-Stokes equation. In Refs. [4,16], the measurements of the Hall resistance in samples in which 2D electrons form a viscous fluid were reported. These experiments were performed on different materials (grapheme and GaAs quantum wells) and for samples of different geometries, but their results turned out to be rather similar: The Hall resistance has an additional size-dependent contribution to the standard Hall resistance. The value of the size-dependent contribution in Ref. [4] was directly related to the coefficient of the Hall viscosity.

In Ref. [41], magnetotransport of interacting 2D electrons in long samples with rough edges was theoretically studied. Using the numerical solution of the kinetic equation, the longitudinal and Hall resistances were calculated for the parameters corresponding to both the ballistic and hydrodynamic regimes of transport. It was shown that, for the samples in which the hydrodynamic regime is realized (the mean free path relative to interparticle collisions is much less than the sample width), the Hall resistance deviates from the standard value by a small negative value.

In Refs. [42–45], the Hall effect was theoretically studied for systems of interacting electrons in long samples in the ballistic regime and transition subregimes between the ballistic and hydrodynamic regimes. A variety of anomalies was predicted: For example, the giant value of the Hall resistance in the ballistic region [44] and a kink and other singularities in the longitudinal and Hall resistances in the transition point [45]. Some of these features have been previously discovered in numerical theory [41].

In Ref. [46], the influence of the near-edge layers of the Poiseuille flow on the Hall effect was studied for a long sample with rough edges. In the layers of widths of the order of the interparticle scattering length, half of the electrons are just reflected from an edge of the sample. Therefore, the flow in such layers is semiballistic. It was described by the full

kinetic equation, in contrast to the rest, the bulk part of the sample, where the hydrodynamic equations were applicable. The description of the near-edge layers was carried out in Ref. [46] according to a method like the one developed in Refs. [47,48]. It was shown in Ref. [46] that the contribution of the near-edge semiballistic layers to the Hall resistance is significant: It is of the same order of magnitude as the contribution from the bulk Hall viscosity term.

D. Subject of this paper

In this paper, we develop a theory of the flow of a 2D electron fluid in high-quality samples with rare macroscopic obstacles (*disks*) in a perpendicular magnetic field. Throughout the paper, it is assumed that the free path of electrons with respect to electron-electron collisions (more precisely, the relaxation length of the shear stress in the fluid) is much smaller than the obstacle size. We develop two approaches.

The first one is hydrodynamic. We consider a long sample with disks and solve the Navier-Stokes equation for 2D fluid hydrodynamics, accounting for the diagonal and nondiagonal (Hall) viscosities. Specific calculations were performed within the effective medium method, which we generalized for the case of a charged fluid in a magnetic field. Following Refs. [32–34], we calculate average characteristics of the flow in the whole sample by consideration of the flow around some disk immersed in an effective medium. The last one, consisting of the fluid and all other disks, provides effective resistance for the flow far from a chosen disk.

We calculate the velocity field around a fixed disk as well as the corresponding longitudinal and Hall resistivities within such a model. Owing to the magnetic field dependence of the diagonal viscosity ν , a strong negative magnetoresistance, like in the Poiseuille flow [17], arises. Within small corrections, the longitudinal resistance does not depend on the boundary conditions at the edges of the disks. The Hall resistance depends on the type of disk edges. In the case of rough edges, it is exactly equal to the standard Hall resistance corresponding to the balance between the magnetic Lorenz force and the electric force in the bulk of the fluid. On the contrary, in the case of smooth disk edges, a correction to the standard Hall resistance which is proportional to the Hall viscosity arises.

The second approach goes beyond hydrodynamics. Indeed, the hydrodynamic equations are derived from the kinetic equation formally assuming that all harmonics of the distribution function starting from the third one relax instantaneously. In fact, the relaxation time of the third harmonic is of the same order as the relaxation time of the second harmonic or even far exceeds it [49]. Thus, the question arises, how would the predictions of the purely hydrodynamic theory change, if the three harmonics were included in the calculations? Additionally, from the analogy with the consideration of Ref. [46], it is obvious that a thin semiballistic layer around the obstacle edges is formed. In this layer, the hydrodynamic approximation is not applicable, and higher harmonics of the distribution function should be considered. Approximation of three harmonics is a step in this direction. We derive a system of 2D quasihydrodynamic equations of the electron fluid from the Boltzmann kinetic equation in the three-harmonic approximation and solve it using the effective medium method.

It turns out that, in addition to the spatial scales l_2, R , and $\lambda_\tau = \sqrt{\nu\tau}$, being characteristic for the hydrodynamic approximation and satisfying the inequality $l_2 \ll R \ll \lambda_\tau$, another scale $\lambda \sim \sqrt{l_2 l_3}$ arises. We demonstrate that the last scale, depending on the relaxation length l_3 , can be greater than l_2 and R but is always smaller than λ_τ . If the inequalities $\lambda \ll R, l_3 \ll R$ are fulfilled, then thin semiballistic layers around disks have the width λ . The corresponding resistivity tensor is equal to the hydrodynamic result with an accuracy of small corrections. If $\lambda \ll R \ll l_3$, then the longitudinal resistivity still coincides with its hydrodynamic value, while the correction to the standard Hall resistivity turns out to be nonhydrodynamic. Finally, if $R \ll \lambda \ll l_3$, then the flow regime becomes nonhydrodynamic: The longitudinal resistivity does not depend on the shear stress relaxation length l_2 but on the length l_3 controlling the relaxation of the ballistic contribution. Herewith, the Hall resistance does not depend on both the relaxation lengths l_2 and l_3 at all and is determined only by the properties of obstacles.

We compare our theoretical results on the longitudinal resistance with the experimental data from Ref. [27] on magnetotransport of high-quality GaAs quantum wells with artificial disklike defects, namely, micron-sized holes made by ion etching. The observed giant negative magnetoresistance of different amplitudes is compared with our results for the cases of the flow via an array of disks with rough or smooth edges. Good agreement between theory and experiment is demonstrated. To describe the experimental data, we used only one fitting parameter, the shear stress relaxation rate $1/\tau_2$. It allows us to describe the shape, width, and amplitude of the observed magnetoresistance curves. Based on the good agreement between theory and experiment, we conclude that flows of 2D electron fluid, like the ones studied in this paper, were realized in the studied structures in Ref. [27].

E. Structure of this paper

Below, for convenience, we describe the structure of the rest of this paper.

In Sec. II A, starting from the Navier-Stokes equations in a linear approximation, we present general rigorous statements and derive equations which are the basis of our further calculations.

In Sec. II B, we briefly describe the effective medium method as applied to the hydrodynamic equations of the 2D electron fluid.

In Sec. II C, we perform exact calculations of the velocity field and the resistivity tensor for the flows via arrays of rough disks (those scatter electrons diffusely) and smooth disks (those reflect them mirrorlike).

In Sec. II D, we calculate fluctuations of the components of the resistivity tensor due to irregularities in the arrangement of the disks. We show that the resistivity fluctuations are much smaller than their mean values.

In Sec. II E, we present and briefly discuss the velocity profile in the vicinity of a disk.

In Sec. III, we derive quasihydrodynamic equations based on the three-harmonic approximation for the distribution function. We solve them for the case of smooth disks within the

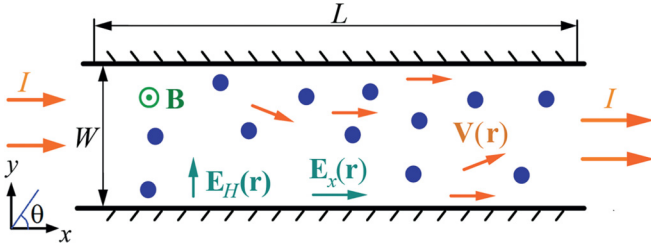


FIG. 1. Long sample with disks and two-dimensional (2D) electron Fermi gas.

effective medium method for different values of the fluid parameters and sizes of disks.

In Sec. IV, we compare our results for the longitudinal resistance with experimental data on magnetoresistance of Ref. [27] of high-quality GaAs quantum well samples in which localized macroscopic obstacles of different densities were fabricated.

In the Conclusions, we sketch all the obtained results and discuss their importance and perspectives.

In the seven appendices, we present derivations of the basic equations used in the main text as well as details of lengthy calculations.

II. HYDRODYNAMIC APPROACH

A. Basis equations

We consider a 2D long sample of length L and width $W \ll L$ located in plane (x, y) and oriented along axis x (see Fig. 1). A homogeneous magnetic field \mathbf{B} is applied in the direction of axis z . It is assumed that the sample contains a degenerate electron gas and that interelectron collisions are the dominant mechanism of electron scattering.

We also suppose that the sample contains macroscopic electron-impermeable obstacles, about which we will assume that they are disks with radius R . The concentration of the disks n_D is assumed to be small enough, namely, the inequality $n_D R^2 \ll 1$ is fulfilled. Throughout this paper, the inequality $l_2 \ll R$ will be assumed to be fulfilled, which allows us to use the hydrodynamic or hydrodynamiclike equations to describe the motion of electron gas. All our results will be obtained in the thermodynamic limit $S = LW \rightarrow \infty$ provided $n_D = \text{const}$.

Our problem is to find the distribution of flow of the electron fluid in the sample and the resistivity tensor of the sample $\rho_{\alpha\beta}$.

We also assume that the perturbation of the electron system caused by the time-independent voltage applied to the sample

is small, which allows us to use the linearized continuity equations and the linearized Navier-Stokes equations to solve the problem:

$$\text{div} \mathbf{V} = 0, \quad e\mathbf{E} + m\omega_c[\mathbf{V} \times \mathbf{e}_z] - m\nu\Delta\mathbf{V} + mv_H[\Delta\mathbf{V} \times \mathbf{e}_z] = 0. \quad (1)$$

Here, $\mathbf{V}(\mathbf{r})$ is the velocity of the electron fluid at the point \mathbf{r} , the symbol $\mathbf{E}(\mathbf{r})$ denotes the gradient of the electrochemical potential $\Psi(\mathbf{r})$ taken with a minus sign, \mathbf{e}_z is a unit vector along the z axis, $\nu = \nu_0/(1 + \beta_2^2)$ is the diagonal viscosity coefficient depending on magnetic field, $\beta_2 = 2\omega_c\tau_2$ is the parameter proportional to magnetic field, $\nu_H = \beta_2\nu$ is the Hall viscosity coefficient, ω_c is the cyclotron frequency, and τ_2 is the relaxation time of the second harmonic of the distribution function, or equivalently, the relaxation time of the shear stress. The value $\Psi(\mathbf{r})$ considers (i) an external bias, (ii) internal electric fields related to the redistribution of 2D electrons due to a nonzero flow, and (iii) a space inhomogeneity of the chemical potential of 2D electrons. The distribution of the disks is considered random and homogeneous, on space scales larger than the average distance between the disks, so that, in sufficiently large samples, the electric field and the electron flow are homogeneous on the same scales.

The first of the equations in Eq. (1) allows us to express the hydrodynamic velocity \mathbf{V} and the vorticity Ω through the flow function ψ :

$$V_x = -\frac{\partial\psi}{\partial y}, \quad V_y = \frac{\partial\psi}{\partial x}, \quad \Omega = \frac{\partial V_y}{\partial x} - \frac{\partial V_x}{\partial y} = \Delta\psi. \quad (2)$$

Introducing the function $e\tilde{\Psi} = e\Psi - mv_H\Omega - m\omega_c\psi$, let us rewrite the Navier-Stokes equations in the form:

$$\frac{\partial\tilde{\Psi}}{\partial x} = -\frac{m\nu}{e}\Delta V_x, \quad \frac{\partial\tilde{\Psi}}{\partial y} = -\frac{m\nu}{e}\Delta V_y, \quad (3)$$

or equivalently:

$$\frac{\partial\tilde{\Psi}}{\partial x} = \frac{m\nu}{e}\frac{\partial\Omega}{\partial y}, \quad \frac{\partial\tilde{\Psi}}{\partial y} = -\frac{m\nu}{e}\frac{\partial\Omega}{\partial x}. \quad (4)$$

By differentiating the first of these equations by y , the second by x , and subtracting the results from each other, we obtain a simple equation for the vorticity $\Delta\Omega = 0$. By virtue of Eq. (2), it is equivalent to the biharmonic equation on the flow function ψ :

$$\Delta^2\psi = 0. \quad (5)$$

By integrating Eq. (4) over the flow area and dividing the result by the sample area S , we obtain

$$\begin{aligned} \frac{1}{S} \int_0^W [\tilde{\Psi}(L, y) - \tilde{\Psi}(0, y)] dy &= \frac{R}{S} \sum_k \oint_{\Gamma_k} \tilde{\Psi} \cos \theta_k d\theta_k - \frac{m\nu R}{eS} \sum_k \oint_{\Gamma_k} \Omega \sin \theta_k d\theta_k + \frac{m\nu}{eS} \int_0^L [\Omega(x, W) - \Omega(x, 0)] dx, \\ \frac{1}{S} \int_0^L [\tilde{\Psi}(x, W) - \tilde{\Psi}(x, 0)] dx &= \frac{R}{S} \sum_k \oint_{\Gamma_k} \tilde{\Psi} \sin \theta_k d\theta_k + \frac{m\nu R}{S} \sum_k \oint_{\Gamma_k} \Omega \cos \theta_k d\theta_k - \frac{m\nu}{eS} \int_0^L [\Omega(L, y) - \Omega(0, y)] dy. \end{aligned} \quad (6)$$

Here, the symbol $\oint_{\Gamma_k} \dots d\theta_k$ means the integration over the edge of the disk with the number k . The lines $x = 0$ and L correspond to the source and drain, respectively. The lines $y = 0$ and W correspond to the lower and upper edges of the sample in the direction of the ordinate axis. The angle θ_k in each summand is counted from the abscissa axis.

From Eq. (5) and the equality $\tilde{E}_\theta = -\partial\tilde{\Psi}/R\partial\theta = mv\partial\Omega/e\partial r$, which follows from Eq. (4), we get

$$\begin{aligned} \frac{1}{S} \int_0^W [\tilde{\Psi}(L, y) - \tilde{\Psi}(0, y)]dy &= \frac{mvR}{eS} \sum_k \oint_{\Gamma_k} \left(R \frac{\partial\Omega}{\partial r} - \Omega \right) \sin\theta d\theta + \frac{mv}{eS} \int_0^L [\Omega(x, W) - \Omega(x, 0)]dx, \\ \frac{1}{S} \int_0^L [\tilde{\Psi}(x, W) - \tilde{\Psi}(x, 0)]dx &= \frac{mvR}{S} \sum_k \oint_{\Gamma_k} \left(-R \frac{\partial\Omega}{\partial r} + \Omega \right) \cos\theta d\theta - \frac{mv}{eS} \int_0^W [\Omega(L, y) - \Omega(0, y)]dy. \end{aligned} \quad (7)$$

Now transferring the functions $-(m\omega_c/e)\psi$ and $-(mv_H/e)\Omega$, included in $\tilde{\Psi}$, from the left parts of these equations to the right ones and introducing the notations U_x and U_y for the differences of electrochemical potentials (voltages), we obtain

$$\begin{aligned} \frac{U_x}{L} &= \frac{mvR}{eS} \sum_k \oint_{\Gamma_k} \left(R \frac{\partial\Omega}{\partial r} - \Omega \right) \sin\theta d\theta + \frac{m\omega_c}{e} \bar{v}_y + \frac{mv}{eS} \int_0^L [\Omega(x, W) - \Omega(x, 0)]dx + \frac{mv_H}{eS} \int_0^W [\Omega(L, y) - \Omega(0, y)]dy, \\ \frac{U_y}{W} &= -\frac{mvR}{eS} \sum_k \oint_{\Gamma_k} \left(R \frac{\partial\Omega}{\partial r} - \Omega \right) \cos\theta d\theta - \frac{m\omega_c}{e} \bar{v}_x - \frac{mv}{eS} \int_0^W [\Omega(L, y) - \Omega(0, y)]dy + \frac{mv_H}{eS} \int_0^L [\Omega(x, W) - \Omega(x, 0)]dx. \end{aligned} \quad (8)$$

In Appendix A, we present details of the derivation of Eq. (8). We show how in these equations appear the velocities averaged over the flow region \bar{V}_x and \bar{V}_y .

The integrals along the edges of the sample in the thermodynamic limit turn to zero. Indeed, the increase of the vorticity Ω with the increase of the sample size would mean an increase in velocity with increasing size, which is obviously not the case. Thus, we obtain

$$\begin{aligned} -m\omega_c \bar{v}_y + \frac{eU_x}{L} - \frac{mvR}{S} \sum_k \oint_{\Gamma_k} \left(R \frac{\partial\Omega}{\partial r} - \Omega \right) \sin\theta d\theta &= 0, \\ m\omega_c \bar{v}_x + \frac{eU_y}{W} + \frac{mvR}{S} \sum_k \oint_{\Gamma_k} \left(R \frac{\partial\Omega}{\partial r} - \Omega \right) \cos\theta d\theta &= 0. \end{aligned} \quad (9)$$

In other words, the transition to these equations is possible only in the case of sufficiently large samples when the contribution to the resistances associated with the edges is small compared with the contribution from the inner region. Equation (9) is the basis for further calculations. Another form of writing these equations, using the momentum flux density tensor, is presented in Sec. III [see Eqs. (46)–(48)].

It is important that Eqs. (5) and (9) do not contain terms with the Hall viscosity. From this fact, we deduce the following statement. In the case when the Hall viscosity ν_H is absent in the boundary conditions on the disk edges, the vorticity Ω also does not depend on the value ν_H according to Eqs. (2) and (5). Therefore, the components of the resistivity tensor also do not depend on ν_H . In Appendix B, we show that, in fact, this statement is true for obstacles of any shape.

It is not difficult to show that the voltages on the disks and on the flow region separately contain contributions proportional to ν_H , but in total, they exactly compensate each other. For this compensation, it is crucial that the flow bypasses around the disks from all sides. To calculate the integral over the interior of the disk, we should account for the potentiality of the electric field. Namely, the integral of the electric field over the curve that lies inside the disk and connects two points on its edge is equal to the integral over the curve that lies outside the disk and connects the same two points.

The statement formulated can be proven just as strongly but more physically. Namely, it is not difficult to show that the work of the force related to the term with the Hall viscosity is zero. The corresponding calculations are performed in Appendix C.

From Eqs. (2) and (5), the second statement also follows: The velocity profile in the sample is independent of the magnetic field if the boundary conditions do not depend on it.

We emphasize that both statements are true only in the case of small amplitudes of flows, when it is possible to discard all nonlinear contributions.

Note that, in a finite-sized sample, there is a small correction to the resistance containing the Hall viscosity. It is given by the integrals at the edges of the sample. In the absence of disks, this correction is responsible for the deviation of the Hall resistance from its standard value in the Poiseuille flow problem.

We conclude this section by a following remark. One can show that, in three-dimensional (3D) bulk flows of electron fluid with disklike 2D symmetry of the 3D flow (columns along axis z , instead of disks), in the absence of a magnetic field, the electron charges are concentrated at the boundaries of the flow region (like in the Hall effect in bulk ohmic conductors). In contrast, from the above equations, it follows that, in the 2D electron flow, the charge density creating the internal electric fields in a 2D sample is distributed over its entire surface (inside disks as well as in the fluid between disks). This means that a 2D electron fluid, unlike a 3D fluid, cannot be considered fully incompressible. Perturbations of the 2D electron density are very small (in the sense of applicability of the equation $\text{div } \mathbf{V} = 0$) but are still important in the above consideration, as they are responsible for the appearance of the internal electric field, particularly the Hall field. Namely, in linear approximation, by the flow magnitude, we can find from Eqs. (1) and (2) the internal electric field $\mathbf{E}(\mathbf{r})$ corresponding to the solution of Eq. (5) for the flow function ψ and the velocity $\mathbf{V}(\mathbf{r})$. Then by solving the integral equation relating the electric field to the charge density, proportional to the perturbation of the electron concentration, we can find the latter.

B. Effective medium method

The exact profile of the fluid flow cannot be calculated for a given arbitrary arrangement of disks in a sample analytically. Therefore, we propose a method of derivation of mean hydrodynamic equations averaged over the positions of disks, that is, over the realizations of disorder. In this derivation, we will follow Refs. [32,39,40], in which the problem of a viscous neutral fluid flowing through an array of randomly placed solid obstacles was considered. It was shown there that, under the condition $n_D R^2 \ll 1$, the problem reduces to describing the fluid flow in a system with one disk immersed in a medium with an effective relaxation time τ simulating the influence of all other disks. The results of these works cannot be transferred directly to the case of a charged fluid, but it is possible to use some ideas expressed there.

First, we average Eq. (9) over the positions of disks, assuming their distribution over the sample to be homogeneous on average and neglecting the contribution of disks close to the edges of the sample. The result is

$$\begin{aligned} -m\omega_c \bar{V}_y + \frac{eU_x}{L} &= mvRn_D \oint_{\Gamma} \left(R \frac{\partial \langle \Omega \rangle_1}{\partial r} - \langle \Omega \rangle_1 \right) \sin \theta d\theta, \\ m\omega_c \bar{V}_x + \frac{eU_y}{W} &= -mvRn_D \oint_{\Gamma} \left(R \frac{\partial \langle \Omega \rangle_1}{\partial r} - \langle \Omega \rangle_1 \right) \cos \theta d\theta, \end{aligned} \quad (10)$$

where the angle brackets with the subscript 1 mean the average value under the condition that one disk (any disk) is fixed, and averaging is performed on the positions of other disks. The values \bar{V}_x and \bar{V}_y will hereafter be considered as given, determined by the given flows of the electron fluid. The voltages are averaged, but we will not put them in the angle brackets for simplification of notation. The method for finding $\langle \Omega \rangle_1$ is set forth below.

The calculations presented in Appendix D lead us to the equation:

$$\begin{aligned} -e\mathbf{E} + mv\Delta\mathbf{V} - mv_H[\Delta\mathbf{V} \times \mathbf{e}_z] - m\omega_c[\mathbf{V} \times \mathbf{e}_z] \\ - m\delta\omega_c[\mathbf{V} \times \mathbf{e}_z] - \frac{m\mathbf{V}}{\tau} = 0, \end{aligned} \quad (11)$$

where τ and $\delta\omega_c$ at $\bar{V}_y = 0$, which is the case in our problem, are given by the expressions:

$$\begin{aligned} \frac{1}{\tau} &= \frac{vRn_D}{\bar{V}_x} \oint_{\Gamma} \left(R \frac{\partial \langle \Omega \rangle_1}{\partial r} - \langle \Omega \rangle_1 \right) \sin \theta d\theta, \\ \delta\omega_c &= \frac{vRn_D}{\bar{V}_x} \oint_{\Gamma} \left(R \frac{\partial \langle \Omega \rangle_1}{\partial r} - \langle \Omega \rangle_1 \right) \cos \theta d\theta. \end{aligned} \quad (12)$$

Such an equation implies that the effective force of the effective medium acting on the fluid can be written in the form:

$$\mathbf{f} = -\frac{m\mathbf{V}}{\tau} - m\delta\omega_c[\mathbf{V} \times \mathbf{e}_z].$$

Let us emphasize that the average local field $\mathbf{E}(\mathbf{r})$ in Eq. (11) includes both the contribution of configurations in which point \mathbf{r} lies in the flow region and the contribution of configurations in which it appears inside one of the disks for the positions of which the averaging is performed.

Applying the rotor operation to Eq. (11), we obtain the equation for $\langle \Omega \rangle_1$:

$$\Delta \langle \Omega \rangle_1 - \frac{1}{\lambda_\tau^2} \langle \Omega \rangle_1 = 0, \quad \lambda_\tau = \sqrt{\nu\tau}, \quad \varepsilon^2 = \frac{R^2}{\lambda_\tau^2}. \quad (13)$$

Here, the parameter ε is small: $\varepsilon \ll 1$. The solution of the first from these equations, however, will not help us since the boundary conditions formulated are not set for vorticity but for velocity, which is not directly expressed by $\langle \Omega \rangle_1$. Since $\Omega = \Delta\psi$, it follows from Eq. (13) (the angle brackets and subscript 1 we hereafter omit):

$$\Delta^2 \psi - \frac{1}{\lambda_\tau^2} \Delta \psi = 0. \quad (14)$$

After solving this equation with proper boundary conditions, we can find $\mathbf{V}(\mathbf{r})$ and $\Omega(\mathbf{r})$ by Eq. (2).

Because of the invariance of Eq. (14) with respect to rotations, it is natural to represent its general solution in the one-disk problem as a sum over harmonics $\exp(im\theta)$. The condition for the velocity field to be homogeneous at infinity requires that $m = \pm 1$. Therefore, we construct the solution being proportional only to these two $m = \pm 1$ harmonics. The general real solution of Eq. (14), containing only these harmonics, is

$$\psi = 2\text{Re} \left\{ \left[\alpha\rho + \frac{\delta}{\rho} + \gamma K_1(\varepsilon\rho) + \mu I_1(\varepsilon\rho) \right] \exp i\theta \right\}, \quad (15)$$

where α , β , γ , and δ are complex constants independent of ρ and θ ; $\rho = \mathbf{r}/R$ is the dimensionless radius vector; and $K_1(x)$ and $I_1(x)$ are the modified Bessel functions. The function $I_1(\varepsilon\rho)$ exponentially increases with the increasing argument, so we put $\mu = 0$. The function $K_1(\varepsilon\rho)$, in contrast, exponentially decreases at large distances. Therefore, we have

$$\psi = 2\text{Re} \left\{ \left[\alpha\rho + \frac{\delta}{\rho} + \gamma K_1(\varepsilon\rho) \right] \exp i\theta \right\}. \quad (16)$$

Since the velocity vector of the fluid at $\rho \rightarrow \infty$ tends to a coordinate-independent value (\bar{V}_x, \bar{V}_y) , according to Eqs. (2) and (16), we get

$$\alpha = \frac{R\bar{V}_y}{2} + i\frac{R\bar{V}_x}{2} \equiv \alpha_1 + i\alpha_2. \quad (17)$$

The radial velocity $V_r = -\partial\psi/r\partial\theta$ at the edge of the disk (at $\rho = 1$) is zero. From this condition and Eq. (16), it follows

$$\begin{aligned} \alpha + \delta + \gamma K_1(\varepsilon) &= 0, \\ \psi &= 2\text{Re} \left\{ \left[\alpha \left(\rho - \frac{1}{\rho} \right) - \gamma \frac{K_1(\varepsilon)}{\rho} + \gamma K_1(\varepsilon\rho) \right] \exp i\theta \right\}. \end{aligned} \quad (18)$$

Substituting this expression into the equality $\Omega = \Delta\psi$, we obtain

$$\Omega(r, \theta) = \frac{\varepsilon^2}{R^2} K_1(\varepsilon\rho) [\gamma \exp(i\theta) + \gamma^* \exp(-i\theta)]. \quad (19)$$

The coefficient γ will be found below from the second boundary condition at the edges of the disks separately for the cases of rough and smooth disks. From Eqs. (12) and (19),

it follows

$$\frac{1}{\tau} = \frac{2\pi v n_D \varepsilon^3 K_2(\varepsilon)}{R V_x} \gamma_2, \quad \delta\omega_c = -\frac{2\pi v n_D \varepsilon^3 K_2(\varepsilon)}{R V_x} \gamma_1, \quad (20)$$

where $\gamma_1 = \text{Re}(\gamma)$ and $\gamma_2 = \text{Im}(\gamma)$. Equation (20) allows us to self-consistently find expressions for the parameters of the effective medium τ and $\delta\omega_c$.

From Eq. (10), we obtain (recall that $\bar{V}_y = 0$)

$$\begin{aligned} \frac{U_x}{L} &= -\frac{2\pi m v n_D \varepsilon^3 K_2(\varepsilon)}{e R} \gamma_2, \\ \frac{U_y}{W} &= -\frac{2\pi m v n_D \varepsilon^3 K_2(\varepsilon)}{e R} \gamma_1 + m \omega_c \bar{V}_x. \end{aligned} \quad (21)$$

Remember that $\varepsilon = R/\lambda_\tau$ depends on τ . From here, we find

$$\begin{aligned} \rho_{xx} &= \frac{2\pi m v n_D \varepsilon^3 K_2(\varepsilon)}{e^2 n_0 R V_x} \gamma_2, \\ \rho_{xy} \equiv \rho_H &= \rho_H^0 + \frac{2\pi m v n_D \varepsilon^3 K_2(\varepsilon)}{e^2 n_0 R V_x} \gamma_1, \quad \rho_H^0 = \frac{B}{e n_0 c}. \end{aligned} \quad (22)$$

In the next section, we will derive from these relations the exact expressions for the components of the resistivity tensor in the limiting cases of rough and smooth disks.

C. Calculation of resistivity tensor

1. Rough disks

In this case, the tangential velocity at the edge of the disk is also zero, so using the expression in Eq. (16) for ψ , the expression in Eq. (17) for α (at $\bar{V}_y = 0$), and the relation for the Bessel function $xK'_1(x) = -K_1(x) - xK_0(x)$, we obtain

$$\gamma_1 = 0, \quad \gamma_2 = \frac{R \bar{V}_x}{\varepsilon K_0(\varepsilon)}, \quad (23)$$

which yields

$$\frac{1}{\tau} = \frac{2\pi v n_D \varepsilon^2 K_2(\varepsilon)}{K_0(\varepsilon)} \approx \frac{4\pi v n_D}{K_0(\varepsilon)}, \quad \delta\omega_c = 0. \quad (24)$$

Here, we use the fact that $\varepsilon^2 K_2(\varepsilon) \approx 2$ at $\varepsilon \ll 1$. From Eqs. (24) and (13), the equation on the parameter ε follows:

$$\varepsilon^2 = \frac{2\pi n_D \varepsilon^2 K_2(\varepsilon) R^2}{K_0(\varepsilon)} \approx \frac{4\pi n_D R^2}{K_0(\varepsilon)}. \quad (25)$$

In the expansion of the function $K_0(\varepsilon)$, we should limit ourselves to the main logarithmic contribution by putting $K_0(\varepsilon) \approx \ln[2/(\varepsilon \exp \gamma_E)] \approx \ln(1/\varepsilon)$, where $\gamma_E \approx 0.58$ is the Euler constant. The next (power) terms in the expression for the function $K_0(\varepsilon)$ are illegitimate since the effective medium method, which we use, is valid only in the main order by a small parameter $n_D R^2$. As a result, from Eq. (24), we find

$$\begin{aligned} \frac{1}{\tau} &\approx \frac{8\pi v n_D}{\ln(A \ln A)} \approx 8\pi v n_D \left[\frac{1}{\ln A} - \frac{\ln(\ln A)}{\ln^2 A} \right], \\ A &= \frac{1}{8\pi n_D R^2} \gg 1. \end{aligned} \quad (26)$$

Finally, we get

$$\begin{aligned} \rho_{xx} &\approx \frac{8\pi m v n_D}{e^2 n_0 \ln(A \ln A)} \approx \frac{8\pi m v n_D}{e^2 n_0} \left[\frac{1}{\ln A} - \frac{\ln(\ln A)}{\ln^2 A} \right], \\ \rho_H &= \rho_H^0. \end{aligned} \quad (27)$$

2. Smooth disks

In this case, the second boundary condition at the disk edge requires that the nondiagonal component of the momentum flux tensor is zero:

$$\Pi_{\theta r} = -m v \left(\frac{\partial V_\theta}{\partial r} + \frac{1}{r} \frac{\partial V_r}{\partial \theta} - \frac{V_\theta}{r} \right) - 2m v_H \frac{\partial V_r}{\partial r} = 0. \quad (28)$$

Note the presence of the Hall viscosity in this boundary condition. Substituting here the expressions for the radial $V_\rho = -\partial\psi/\partial\theta$ and tangential $V_\theta = \partial\psi/\partial\rho$ velocity components and considering the expression in Eq. (19) for the function ψ , we obtain

$$\gamma = \frac{4\alpha(1 + i\beta_2)}{\varepsilon[2(1 + i\beta_2)K_0(\varepsilon) + \varepsilon K_1(\varepsilon)]}. \quad (29)$$

From this equation and the formulas in Eq. (20), it follows

$$\begin{aligned} \frac{1}{\tau} &= \frac{4\pi v n_D \varepsilon^2 K_2(\varepsilon)[2K_0(\varepsilon)(1 + \beta_2^2) + \varepsilon K_1(\varepsilon)]}{[2K_0(\varepsilon) + \varepsilon K_1(\varepsilon)]^2 + 4\beta_2^2 K_0^2(\varepsilon)} \approx \frac{4\pi n_D v}{K_0(\varepsilon)}, \\ \delta\omega_c &\approx \frac{4\pi n_D \varepsilon^2 K_2(\varepsilon) \varepsilon K_1(\varepsilon) v_H}{[2K_0(\varepsilon) + \varepsilon K_1(\varepsilon)]^2 + 4\beta_2^2 K_0^2(\varepsilon)} \approx \frac{2\pi n_D v_H}{K_0^2(\varepsilon)(1 + \beta_2^2)}, \end{aligned} \quad (30)$$

and the equation for the parameter ε :

$$\varepsilon^2 = \frac{4\pi n_D R^2 \varepsilon^2 K_2(\varepsilon)[2K_0(\varepsilon)(1 + \beta_2^2) + \varepsilon K_1(\varepsilon)]}{[2K_0(\varepsilon) + \varepsilon K_1(\varepsilon)]^2 + 4\beta_2^2 K_0^2(\varepsilon)} \approx \frac{4\pi R^2 n_D}{K_0(\varepsilon)}. \quad (31)$$

Here, we have omitted small corrections since the parameter ε enters the expressions for the resistivities only under the logarithmic sign. Finally, for the resistivity tensor, we obtain the result (up to the inverse square of the large logarithm):

$$\rho_{xx} \approx \frac{8\pi m v n_D}{e^2 n_0} \left[\frac{1}{\ln A} - \frac{\ln(\ln A)}{\ln^2 A} - \frac{v^2}{(v^2 + v_H^2) \ln^2 A} \right], \quad (32)$$

$$\rho_H \approx \rho_H^0 + \frac{8\pi m n_D v^2 v_H}{e^2 n_0 (v^2 + v_H^2) \ln^2 A}. \quad (33)$$

Here, we see an appearance of the correction to the standard Hall resistance, as we announced in Sec. II.

Note that the expressions for ρ_{xx} in the cases of the rough and smooth disks differ only by the corrections, being small by the inverse square of the large logarithm. If we neglect these corrections, we will have in both cases the following dependence of resistivity on the magnetic field:

$$\rho_{xx} = \frac{m}{e^2 n_0 \tau} \approx \frac{8\pi m n_D v}{e^2 n_0 \ln(1/4\pi n_D R^2)},$$

qualitatively coinciding with the experimental one (see Sec. IV). It is important that the disk radius enters this expression only under the sign of the logarithm. One can show that the appearance of the logarithmic dependence here is related to the so-called Stokes paradox.

It can be seen from the expression for ρ_{xx} that the characteristic relaxation time of the flow velocity τ is of the order of the momentum diffusion time by the distance $d \sim \sqrt{\ln A/n_D}$: $\tau \sim d^2/\nu$ (we recall that the viscosity coefficient ν has the meaning of the momentum diffusion coefficient).

D. Corrections to self-consistent results due to fluctuations in location of disks

In the previous sections, we have considered values averaged over realizations. Now let us discuss the role of fluctuations in arrangements of disks, which we will consider random, so that a typical fluctuation of the number of disks in a region containing N disks is \sqrt{N} . Let us first discuss in detail the resistance fluctuations in the absence of a magnetic field and, second, briefly describe the Hall resistance fluctuations.

Within the framework of the effective medium method, we calculated the rate τ^{-1} , standing on one of the disks and replacing all other disks by a homogeneous medium with the mean effective momentum relaxation time. It turned out that the result is determined by disks located inside the circle of the radius $R_\varepsilon = R/\varepsilon = \sqrt{\nu\tau}$. On average, there are $N_\varepsilon = n_D\nu\tau \sim \ln A$ disks in this circle with a concentration equal to $n_D = N_\varepsilon/S_\varepsilon$, where $S_\varepsilon = \pi R_\varepsilon^2$. The typical deviation of the number of disks in this region from its mean value is of the order of $\sqrt{N_\varepsilon} \sim \sqrt{\ln A}$, whence it follows for the concentration fluctuation: $\delta n_D \sim \pm n_D/\sqrt{\ln A}$. According to Eq. (22), we estimate the inverse time τ^{-1} fluctuation caused

by this density fluctuation as

$$\delta\tau^{-1} \approx \frac{\nu\delta n_D}{\ln A} + \frac{\nu\delta n_D}{\ln^2(1/n_D R^2)} \approx \pm \frac{\nu n_D}{\ln^{3/2} A}.$$

Now using the formula from Ref. [49]:

$$\delta\rho \sim \frac{\langle(\delta\tau^{-1})^2\rangle}{\tau^{-1}},$$

we obtain the typical deviation of the resistivity of a sample from its average value:

$$\delta\rho_{xx} \sim \frac{\rho_{xx}}{\ln A} \ll \rho_{xx}. \quad (34)$$

In the case of smooth disks, similar estimates of the contribution of fluctuations to the correction to the Hall resistivity $\Delta\rho_H$ yield

$$\delta(\Delta\rho_H) \sim \frac{\Delta\rho_H}{\ln A} \ll \Delta\rho_H. \quad (35)$$

In this way, the fluctuations of the value $\Delta\rho_H$ are indeed small as compared with its mean value.

E. Electron fluid velocity in the vicinity of disks

In this section, we discuss the velocity field near a fixed disk and briefly touch on the problem of finding the electric field. Using the first two formulas in Eq. (2), the expression in Eq. (16) for ψ , and the fact that, in our problem, $\vec{V}_y = 0$, we obtain $\alpha_1 = 0$ and

$$V_x = \frac{2}{R} \left\{ \alpha_2 - \frac{\varepsilon\gamma_2 K_0(\varepsilon\rho)}{2} + \left[\gamma_2 S(\rho) - \frac{\alpha_2}{\rho^2} \right] \cos 2\theta + \gamma_1 S(\rho) \sin 2\theta \right\},$$

$$V_y = \frac{2}{R} \left\{ -\frac{\gamma_1 \varepsilon K_0(\varepsilon\rho)}{2} - \gamma_1 S(\rho) \cos 2\theta + \left[\gamma_2 S(\rho) - \frac{\alpha_2}{\rho^2} \right] \sin 2\theta \right\}, \quad S(\rho) = \frac{\varepsilon K_0(\varepsilon\rho)}{2} + \frac{K_1(\varepsilon\rho)}{\rho} - \frac{K_1(\varepsilon)}{\rho^2}.$$

Hence, for the case of rough disks, when γ is given by the expression in Eq. (19) and $\gamma_1 = 0$, it follows from the above equations:

$$V_x = \bar{V}_x \left(-1 + \frac{K_0(\varepsilon\rho)}{K_0(\varepsilon)} + \left\{ \frac{K_0(\varepsilon\rho)}{K_0(\varepsilon)} - \frac{1}{\rho^2} + \frac{2}{\varepsilon K_0(\varepsilon)} \left[\frac{K_1(\varepsilon\rho)}{\rho} - \frac{K_1(\varepsilon)}{\rho^2} \right] \right\} \cos 2\theta \right),$$

$$V_y = \bar{V}_x \left\{ \frac{K_0(\varepsilon\rho)}{K_0(\varepsilon)} - \frac{1}{\rho^2} + \frac{2}{\varepsilon K_0(\varepsilon)} \left[\frac{K_1(\varepsilon\rho)}{\rho} - \frac{K_1(\varepsilon)}{\rho^2} \right] \right\} \sin 2\theta.$$

From these expressions, in the domain $\varepsilon\rho \ll 1$, we obtain with the logarithmic accuracy:

$$V_x \approx \frac{\bar{V}_x}{\ln[4/(\varepsilon^2 \exp 2\gamma_E)]} \left[\ln \rho^2 + \left(1 - \frac{1}{\rho^2} \right) \cos 2\theta \right],$$

$$V_y \approx \frac{\bar{V}_x}{\ln[4/(\varepsilon^2 \exp 2\gamma_E)]} \left(1 - \frac{1}{\rho^2} \right) \sin 2\theta.$$

These expressions mean that the velocity profile is, on average, symmetrical about an axis passing through the center of a disk and parallel to the abscissa axis (see Fig. 2).

It is seen from the above expressions for the velocity components that, according to the second statement in Sec. II B, the velocity profile (at given value \bar{V}_x) does not depend on the

magnetic field. Indeed, according to Eq. (25), the value ε^2 is only a function of $n_D R^2$.

Similarly, it is not difficult to find V_x and V_y in the case of smooth disks. The resulting expressions are too cumbersome, and we do not present them. Let us only note that the approximation in Eq. (25) is too crude for γ_2 , and we should use the

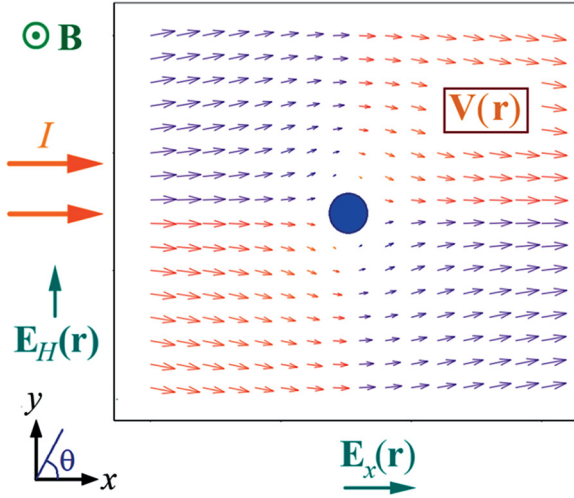


FIG. 2. Profile of the hydrodynamic velocity of the electron fluid near a rough disk. Size of the plot is $16R$.

formula:

$$\gamma_2 \approx \frac{2\alpha_2}{\varepsilon K_0(\varepsilon)} - \frac{2\alpha_2}{4\varepsilon K_0^2(\varepsilon)(1 + \beta_2^3)}.$$

Indeed, in the approximation in Eq. (25) and in the absence of a magnetic field, we get the same expressions for velocity as in the case of rough disks and, therefore, $\mathbf{V} = 0$ at the edge of the disk, which is not true. The velocity field now directly depends on the magnetic field, and at $B \neq 0$, there is no symmetry with respect to the abscissa axis.

Knowing the velocity profile, we can find the distribution of the electric field $\mathbf{E}(\mathbf{r})$ everywhere in the region of the flow from the Navier-Stokes Eq. (1) for both cases of rough and smooth disks.

III. BEYOND STANDARD HYDRODYNAMICS

In this section, we present a theory that goes beyond the hydrodynamics described above in the sense of a complication of the type of distribution of electrons by velocities in a flow.

There are two reasons for such a consideration (both were formulated in the Introduction).

First, the Navier-Stokes equation is derived from the kinetic equation under the assumption that all harmonics of the distribution function, starting from the third harmonic, relax instantaneously. In fact, the relaxation time of the third harmonic is of the same order as the relaxation time of the second harmonic, $\tau_2 \sim \tau_3$, or even much longer than it: $\tau_2 \ll \tau_3$ [50]. In the latter case, $\tau_4 \approx \tau_2$ and $\tau_5 \approx \tau_3$, and the influence of the slow-relaxing third harmonic terms may be substantial. According to Appendix E, each of the amplitudes of the distribution functions $f_{ns,c}$ is related only to the amplitudes $f_{n\pm 1s,c}$, whence and from the above relations between τ_m it follows that the influence of the harmonics $f_{4s,c}$, $f_{5s,c}$, and so on, on the values of harmonics $f_{1s,c}$, $f_{2s,c}$, and $f_{3s,c}$ is rapidly decreasing, and thus, $f_{4s,c}$, $f_{5s,c}$... are far less substantial than the role of the third harmonics. In this way, the question arises, how will the predictions of the theory change, if the three harmonics are included in the calculations (and higher ones are neglected)?

Second, it is obvious in advance that there is some layer near the obstacle edges where electrons can be scattered on the obstacle edges; therefore, the hydrodynamic approximation is inapplicable there, and the flow in these layers is semiballistic. In these regions, it is necessary to consider higher harmonics of the distribution function. Approximation by three harmonics is a step toward this direction. We limited ourselves to the case of smooth disks because, in the hydrodynamic approach, exactly in this case, there appears a nontrivial correction to the standard Hall resistance, proportional to the Hall viscosity ν_H , and it is interesting to see how it will change due to accounting for the third harmonic terms, being a rough description of the semiballistic character of the flow.

A. Basis equations

We start our consideration from the derivation of the exact equations for the momentum flux density tensor $\Pi_{ik}(\mathbf{r})$.

Let us write the kinetic equation in the form:

$$\text{div}(f\mathbf{v}) - e\mathbf{E}(\mathbf{r})\frac{\partial f}{\partial \mathbf{p}} + \omega_c \frac{\partial f}{\partial \phi} = St_{ee}(f), \quad e > 0. \quad (36)$$

By representing the function $f(\mathbf{p}, \mathbf{r})$ in the form of $f = f_0(\varepsilon, \mathbf{r}) + \tilde{f}(\varepsilon, \phi, \mathbf{r})$, $\int_0^{2\pi} \tilde{f} d\phi = 0$, multiplying Eq. (36) by p_y , and by integrating the result with $2d^2\mathbf{p}/(2\pi\hbar)^2$, we obtain

$$\begin{aligned} \frac{\partial \bar{\varepsilon}(\mathbf{r})}{\partial y} + en(\mathbf{r})E_y(\mathbf{r}) + n_0 \frac{\partial \Pi_{yx}(\mathbf{r})}{\partial x} \\ + n_0 \frac{\partial \Pi_{yy}(\mathbf{r})}{\partial y} - m\omega_c V_x(\mathbf{r})n(\mathbf{r}) = 0, \end{aligned} \quad (37)$$

where

$$\begin{aligned} \bar{\varepsilon}(\mathbf{r}) &\equiv \int f_0(\varepsilon, \mathbf{r}) \varepsilon \frac{2d^2\mathbf{p}}{(2\pi\hbar)^2}, \\ \Pi_{ik}(\mathbf{r}) &\equiv \frac{m}{n_0} \int \tilde{f} v_i v_k \frac{2d^2\mathbf{p}}{(2\pi\hbar)^2}, \\ V_i(\mathbf{r}) &= \frac{1}{n(\mathbf{r})} \int \tilde{f}(\mathbf{p}, \mathbf{r}) v_i \frac{2d^2\mathbf{p}}{(2\pi\hbar)^2}, \end{aligned}$$

where $n(\mathbf{r})$ is the concentration of electrons, n_0 is the equilibrium concentration, $\bar{\varepsilon}(\mathbf{r})$ is the energy density of the electron gas, and $\Pi_{ik}(\mathbf{r})$ is viscous stress tensor. We recall that, in the case of interparticle collisions, there is an equality $\int St_{ee}(f)\mathbf{v}d^2\mathbf{p} = 0$. Similarly, we obtain the equation:

$$\begin{aligned} \frac{\partial \bar{\varepsilon}(\mathbf{r})}{\partial x} + en(\mathbf{r})E_x(\mathbf{r}) + n_0 \frac{\partial \Pi_{xx}(\mathbf{r})}{\partial x} \\ + n_0 \frac{\partial \Pi_{xy}(\mathbf{r})}{\partial y} + m\omega_c V_y(\mathbf{r})n(\mathbf{r}) = 0. \end{aligned} \quad (38)$$

Note that Eqs. (37) and (38) are exact. They can be conveniently rewritten in the form:

$$\begin{aligned} enE_x + \frac{\partial \bar{\varepsilon}}{\partial x} + n_0 \text{div} \Pi_x + mn\omega_c V_y = 0, \\ enE_y + \frac{\partial \bar{\varepsilon}}{\partial y} + n_0 \text{div} \Pi_y - mn\omega_c V_x = 0, \end{aligned} \quad (39)$$

$$\Pi_i(\mathbf{r}) \equiv \frac{m}{n_0} \int \tilde{f} v_i \mathbf{v} \frac{2d^2\mathbf{p}}{(2\pi\hbar)^2}.$$

Throughout this paper, we assume that the screening length is smaller than all other spatial scales of the problem; therefore, in absence of a current, the electric field is zero. Correspondingly, in the last case, the concentration and the density of the energy of electrons are the same everywhere. If the electric field applied to the sample is small, we linearize Eq. (39), which yields

$$\begin{aligned} eE_x + \frac{1}{n_0} \frac{\partial \bar{\varepsilon}}{\partial x} + \text{div} \mathbf{\Pi}_x + m\omega_c V_y &= 0, \\ eE_y + \frac{1}{n_0} \frac{\partial \bar{\varepsilon}}{\partial y} + \text{div} \mathbf{\Pi}_y - m\omega_c V_x &= 0. \end{aligned} \quad (40)$$

Now we introduce the electric ϕ and the electrochemical $\Psi = \phi - \bar{\varepsilon}/en_0$ potentials. Equation (41) is now written in the form:

$$\frac{\partial \Psi}{\partial x} = \frac{1}{e} \text{div} \mathbf{\Pi}_x + \frac{B}{c} V_y, \quad \frac{\partial \Psi}{\partial y} = \frac{1}{e} \text{div} \mathbf{\Pi}_y - \frac{B}{c} V_x. \quad (41)$$

By integrating these equations over the flow domain, we obtain the following expressions for the longitudinal and Hall voltages:

$$\begin{aligned} U_{sd} &\equiv \frac{1}{W} \int_0^W [\Psi(L, y) - \Psi(0, y)] dy \\ &= \frac{L}{eS} \sum_j \oint_{\Gamma_j} d\mathbf{l}_j \cdot \mathbf{\Pi}_x + \frac{RL}{S} \sum_j \oint_{\Gamma_j} \Psi(\theta, R) \cos \theta d\theta, \\ U_H &\equiv \frac{1}{L} \int_0^L [\Psi(x, W) - \Psi(x, 0)] dx \\ &= \frac{W}{eS} \sum_j \oint_{\Gamma_j} d\mathbf{l}_j \cdot \mathbf{\Pi}_y + \frac{RW}{S} \sum_j \oint_{\Gamma_j} \Psi(\theta, R) \sin \theta d\theta \\ &\quad + \frac{BI}{en_0 c}, \end{aligned} \quad (42)$$

where θ is the polar angle vector pointing from the center of this disk to its edge. Also remember that we assume $\bar{V}_y = 0$ and omit the integrals on the edges of the sample. Equivalently, Eq. (42) can be written via the effective electric field E_θ :

$$\begin{aligned} U_{sd} &= \frac{L}{eS} \sum_j \oint_{\Gamma_j} d\mathbf{l}_j \cdot \mathbf{\Pi}_x + \frac{R^2 L}{S} \sum_j \oint_{\Gamma_j} E_\theta \sin \theta d\theta, \\ U_H &= \frac{BI}{en_0 c} + \frac{W}{eS} \sum_j \oint_{\Gamma_j} d\mathbf{l}_j \cdot \mathbf{\Pi}_y \\ &\quad - \frac{R^2 W}{S} \sum_j \oint_{\Gamma_j} E_\theta \cos \theta d\theta, \end{aligned} \quad (43)$$

Here, the symbol E_θ denotes the value $-\partial\Psi/R\partial\theta$, and $d\mathbf{l}_j$ is the vector of the disk boundary element pointing to its center. The first terms in the right-hand sides of Eq. (43) are equal

to the voltage drop on the flow region, and the last terms are equal to the voltage drop on the disks.

Let us transform the second equation in Eq. (43). Since $d\mathbf{l}_j \cdot \mathbf{\Pi}_y = -\Pi_{yr} R d\theta$ and $v_y = v_r \sin \theta + v_\theta \cos \theta$, the contribution of the flow region will be written as

$$\begin{aligned} \frac{W}{eS} \sum_j \oint_{\Gamma_j} d\mathbf{l}_j \cdot \mathbf{\Pi}_y &= -\frac{RW}{eS} \sum_j \oint_{\Gamma_j} (\Pi_{rr} \sin \theta \\ &\quad + \Pi_{\theta r} \cos \theta) d\theta. \end{aligned} \quad (44)$$

We consider that, due to the condition $\int_0^{2\pi} \tilde{f}(\varepsilon, \phi, \mathbf{r}) d\phi = 0$, the relations $\Pi_{yy} = -\Pi_{xx}$, $\Pi_{\theta\theta} = -\Pi_{rr}$ are fulfilled, and the equalities $V_x \cos \theta + V_y \sin \theta = V_r$, $\partial\Psi/\partial\theta = R \cos \theta \partial\Psi/\partial y - R \sin \theta \partial\Psi/\partial x$, and $V_r(\mathbf{r})|_{r=R} = 0$ are valid. After cumbersome but elementary calculations, we obtain from these relations and Eq. (41)

$$E_\theta = -\frac{1}{e} \left(\frac{\partial \Pi_{r\theta}}{\partial r} + \frac{2}{r} \Pi_{r\theta} - \frac{1}{r} \frac{\partial \Pi_{rr}}{\partial \theta} \right). \quad (45)$$

Substituting Eqs. (44) and (45) into the formula in Eq. (43), we obtain for the Hall voltage

$$U_H = \frac{BI}{en_0 c} + \frac{RW}{eS} \sum_j \oint_{\Gamma_j} \left(\frac{\partial \Pi_{r\theta}}{\partial \rho} - 2 \frac{\partial \Pi_{rr}}{\partial \theta} \right)_{\rho=1} \cos \theta d\theta, \quad (46)$$

or after averaging over the positions of the disks:

$$U_H = \frac{BI}{en_0 c} + \frac{RW n_D}{e} \oint_{\Gamma} \left(\frac{\partial \Pi_{r\theta}}{\partial \rho} - 2 \frac{\partial \Pi_{rr}}{\partial \theta} \right)_{\rho=1} \cos \theta d\theta. \quad (47)$$

Similarly, for the source-drain voltage, we get

$$U_{sd} = -\frac{RL}{eS} \sum_j \int_{\Gamma_j} \left(\frac{\partial \Pi_{r\theta}}{\partial \rho} - 2 \frac{\partial \Pi_{rr}}{\partial \theta} \right)_{\rho=1} \sin \theta d\theta.$$

Within the effective-media approach, this yields

$$U_{sd} = -\frac{RL n_D}{e} \int_{\Gamma} \left(\frac{\partial \Pi_{r\theta}}{\partial \rho} - 2 \frac{\partial \Pi_{rr}}{\partial \theta} \right)_{\rho=1} \sin \theta d\theta. \quad (48)$$

In the derivation of the expressions in Eqs. (47) and (48), it was considered that, at the edge of the disk, the condition $\Pi_{r\theta} = 0$ takes place. We will also need the last expression in the future consideration.

Our approach of description of the ballistic effects is based on using a truncated representation of the generalized distribution function $\tilde{f}(\mathbf{r}, \phi)$ as a sum over three angular harmonics:

$$\tilde{f}(\mathbf{r}, \phi) = \sum_{m=1}^3 [f_{mc}(\mathbf{r}) \cos(m\phi) + f_{ms}(\mathbf{r}) \sin(m\phi)]. \quad (49)$$

Such a form of f leads to the following system of the quasihydrodynamic motion equations of the electron fluid (for their derivation, see Appendix E):

$$\begin{aligned} \frac{\partial \Pi_{xx}}{\partial x} + \frac{\partial \Pi_{xy}}{\partial y} + eE_x + m\omega_c V_y &= 0, \quad \frac{\partial \Pi_{yx}}{\partial x} + \frac{\partial \Pi_{yy}}{\partial y} + eE_y - m\omega_c V_x = 0, \\ \frac{\partial V_x}{\partial x} + \frac{\partial V_y}{\partial y} &= 0, \quad \Pi_{yy} = -\Pi_{xx}, \quad \Pi_{yx} = \Pi_{xy}, \end{aligned}$$

$$\begin{aligned}\Pi_{yx} &= -m\nu\left(\frac{\partial V_x}{\partial y} + \frac{\partial V_y}{\partial x}\right) - m\nu_H\left(\frac{\partial V_x}{\partial x} - \frac{\partial V_y}{\partial y}\right) + \frac{\nu\tau_3}{1+\beta_3^2}(\Delta\Pi_{xy} + \beta_3\Delta\Pi_{xx}) + \frac{\nu_H\tau_3}{1+\beta_3^2}(\Delta\Pi_{xx} - \beta_3\Delta\Pi_{xy}), \\ \Pi_{xx} &= -m\nu\left(\frac{\partial V_x}{\partial x} - \frac{\partial V_y}{\partial y}\right) + m\nu_H\left(\frac{\partial V_x}{\partial y} + \frac{\partial V_y}{\partial x}\right) - \frac{\nu_H\tau_3}{1+\beta_3^2}(\Delta\Pi_{xy} + \beta_3\Delta\Pi_{xx}) + \frac{\nu\tau_3}{1+\beta_3^2}(\Delta\Pi_{xx} - \beta_3\Delta\Pi_{xy}).\end{aligned}\quad (50)$$

It is impossible to solve these equations in a general form; however, it can be done in two special cases, namely, in the case of the Poiseuille flow in a long sample with rough edges and in the case of the flow in a sample with many arbitrary distributed disks. In both cases, the variables describing the flow can be separated, as they were in ordinary hydrodynamics. The first of these problems is considered in Ref. [46]. The second one will be discussed below in the framework of the effective medium method.

In this method, instead of the first two equations in Eq. (50), one should use the analogous equation with the introduced effective relaxation time τ and the cyclotron frequency shift $\delta\omega_c$, as in the case of the hydrodynamic Eq. (8):

$$\frac{\partial\Pi_{xx}}{\partial x} + \frac{\partial\Pi_{xy}}{\partial y} + eE_x + m(\omega_c + \delta\omega_c)V_y = -\frac{mV_x}{\tau}, \quad (51a)$$

$$\frac{\partial\Pi_{yx}}{\partial x} + \frac{\partial\Pi_{yy}}{\partial y} + eE_y - m(\omega_c + \delta\omega_c)V_x = -\frac{mV_y}{\tau}, \quad (51b)$$

or equivalently:

$$\begin{aligned}\frac{\partial\Pi_{xx}}{\partial x} + \frac{\partial\Pi_{xy}}{\partial y} - \frac{\partial\Phi}{\partial x} &= \frac{m}{\tau} \frac{\partial\psi}{\partial y}, \\ \frac{\partial\Pi_{yx}}{\partial x} + \frac{\partial\Pi_{yy}}{\partial y} - \frac{\partial\Phi}{\partial y} &= -\frac{m}{\tau} \frac{\partial\psi}{\partial x}, \\ \Phi &= e\Psi - m(\omega_c + \delta\omega_c)\psi.\end{aligned}\quad (52)$$

Applying of the rotor operator to Eq. (52) yields

$$2\frac{\partial^2\Pi_{xx}}{\partial y\partial x} + \frac{\partial^2\Pi_{xy}}{\partial^2y} - \frac{\partial^2\Pi_{xy}}{\partial^2x} = \frac{m}{\tau}\Delta\psi.$$

By substituting here the expressions in Eq. (50) for Π_{ik} and using Eq. (52), we obtain

$$\left[m\nu + \frac{m\xi^2}{\tau}(1 - \beta_2\beta_3)\right]\Delta^2\psi - \xi^2(\beta_2 + \beta_3)\Delta^2\Phi = \frac{m}{\tau}\Delta\psi, \quad \xi = \sqrt{\frac{\nu\tau_3}{(1 + \beta_3^2)}}. \quad (53)$$

Applying the divergence operator to Eq. (51b) and performing similar calculations, we obtain another equation for the functions Φ and ψ :

$$m\beta_2\nu\Delta^2\psi + \xi^2(1 - \beta_2\beta_3)\Delta^2\Phi - \Delta\Phi = 0.. \quad (54)$$

Equations (53) and (54) can be written as

$$\begin{aligned}\frac{\beta_2 + \beta_3}{(1 + \beta_2^2)m\nu}\Delta\Phi &= \left[1 + \frac{\lambda^2(1 - \beta_2\beta_3)^2}{\lambda_\tau^2(1 + \beta_2^2)^2}\right]\Delta^2\psi - \frac{1 - \beta_2\beta_3}{\lambda_\tau^2(1 + \beta_2^2)}\Delta\psi, \\ \frac{m\beta_2}{\tau}\Delta\psi &= -\lambda^2\left[1 + \frac{\lambda^2(1 - \beta_2\beta_3)^2}{\lambda_\tau^2(1 + \beta_2^2)^2}\right]\Delta^2\Phi + \left(1 + \frac{\lambda^2}{\lambda_\tau^2} \frac{1 - \beta_2\beta_3}{1 + \beta_2^2}\right)\Delta\Phi,\end{aligned}\quad (55)$$

where

$$\lambda^2 = \xi^2(1 + \beta_2^2) = \frac{\nu_0\tau_3}{1 + \beta_3^2} = \frac{l_2l_3}{4(1 + \beta_3^2)}, \quad \nu_0 = \nu(0), \quad \lambda_\tau^2 = \nu\tau.$$

Now expressing $\Delta\Phi$ from the first equation and substituting it into the second as well as expressing from the second equation $\Delta\psi$ and substituting in the first, we get two identical equations for the potentials ψ and Φ :

$$\begin{aligned}\lambda^2\left[1 + \frac{\lambda^2}{\lambda_\tau^2} \frac{(1 - \beta_2\beta_3)^2}{(1 + \beta_2^2)^2}\right]\Delta^3\psi - \left(1 + \frac{2\lambda^2}{\lambda_\tau^2} \frac{1 - \beta_2\beta_3}{1 + \beta_2^2}\right)\Delta^2\psi + \frac{1}{\lambda_\tau^2}\Delta\psi &= 0, \\ \lambda^2\left[1 + \frac{\lambda^2}{\lambda_\tau^2} \frac{(1 - \beta_2\beta_3)^2}{(1 + \beta_2^2)^2}\right]\Delta^3\Phi - \left(1 + \frac{2\lambda^2}{\lambda_\tau^2} \frac{1 - \beta_2\beta_3}{1 + \beta_2^2}\right)\Delta^2\Phi + \frac{1}{\lambda_\tau^2}\Delta\Phi &= 0.\end{aligned}\quad (56)$$

We conclude this subsection by deriving the boundary conditions at the edge of a smooth disk. The mirrorlike reflection of electrons from the disk boundary means that the distribution function is symmetric at the reflection with respect to the tangent

to this boundary:

$$\tilde{f}(\varepsilon, \phi, R, \theta) = \tilde{f}(\varepsilon, \pi + 2\theta - \phi, R, \theta). \quad (57)$$

From this condition for f , we can obtain the following two conditions for Π (they are derived in Appendix F):

$$\Pi_{r\theta}|_{r=R} = 0, \quad \left(-\frac{\partial \Pi_{rr}}{\partial r} + \frac{2\Pi_{rr}}{r} + \frac{1}{r} \frac{\partial \Pi_{r\theta}}{\partial \theta} \right)_{r=R} + \beta_3 \left(\frac{\partial \Pi_{r\theta}}{\partial r} + \frac{1}{r} \frac{\partial \Pi_{rr}}{\partial \theta} - \frac{2\Pi_{r\theta}}{r} \right)_{r=R} = 0. \quad (58)$$

The first of these conditions is accurate, while the second, as can be seen from Appendix D, is approximate: It does not consider the contribution of the fourth harmonic.

B. Solution of equations for ψ and Φ around one disk

Equation (56) can be solved by the decomposition of the differential operator as a product of three commuting differential operators as follows:

$$\Delta(\Delta - \kappa_+)(\Delta - \kappa_-)\psi = 0, \quad (59)$$

where κ_{\pm} are roots of the equation:

$$\lambda^2 \left[1 + \frac{\lambda^2 (1 - \beta_2 \beta_3)^2}{\lambda_{\tau}^2 (1 + \beta_2^2)^2} \right] \kappa^2 - \left(1 + \frac{2\lambda^2 (1 - \beta_2 \beta_3)}{\lambda_{\tau}^2 (1 + \beta_2^2)} \right) \kappa + \frac{1}{\lambda_{\tau}^2} = 0. \quad (60)$$

With corrections of the order of $\lambda^2/\lambda_{\tau}^2$, the values κ_{\pm} have the forms $\kappa_+ = 1/\lambda^2$ and $\kappa_- = 1/\lambda_{\tau}^2$. Bearing in mind that we are interested in the first-order harmonic of the function ψ , the operator in the left part of Eq. (59) can be written as the product of three radial differential operators:

$$\Delta_r(\Delta_r - \kappa_+)(\Delta_r - \kappa_-)\chi = 0, \quad (61)$$

where χ is the absolute value of ψ , $\psi = 2\text{Re}[\chi \exp(i\theta)]$, and

$$\Delta_r = \frac{1}{r} \frac{d}{dr} \left(r \frac{d}{dr} \right) - \frac{1}{r^2}$$

is the radial part of the Laplace operator. The solution of Eq. (61) is the sum of the solutions of the three differential equations:

$$\Delta_r \chi = 0, \quad (\Delta_r - \kappa_+) \chi = 0, \quad (\Delta_r - \kappa_-) \chi = 0.$$

Such a sum can be presented as

$$\begin{aligned} \chi &= \alpha r + \frac{\delta}{r} + \gamma_+ K_1(\sqrt{\kappa_+} r) + \gamma_- K_1(\sqrt{\kappa_-} r) \\ &\approx \alpha r + \frac{\delta}{r} + \gamma_+ K_1\left(\frac{r}{\lambda}\right) + \gamma_- K_1\left(\frac{r}{\lambda_{\tau}}\right). \end{aligned} \quad (62)$$

Similarly, putting $\Phi = 2\text{Re}[\varphi \exp(i\theta)]$, we have

$$\begin{aligned} \varphi &= \tilde{\alpha} r + \frac{\tilde{\delta}}{r} + \tilde{\gamma}_+ K_1(\sqrt{\kappa_+} r) + \tilde{\gamma}_- K_1(\sqrt{\kappa_-} r) \\ &\approx \tilde{\alpha} r + \frac{\tilde{\delta}}{r} + \tilde{\gamma}_+ K_1\left(\frac{r}{\lambda}\right) + \tilde{\gamma}_- K_1\left(\frac{r}{\lambda_{\tau}}\right). \end{aligned} \quad (63)$$

In the expressions in Eqs. (62) and (63), we omit the exponentially increasing terms.

By virtue of Eq. (55), the coefficients in front of the cylindrical functions are not independent. Substituting the functions $\tilde{\gamma}_- K_1(\sqrt{\kappa_-} r)$, $\gamma_- K_1(\sqrt{\kappa_-} r)$ into the first equation in Eq. (55) and considering that $\Delta K_1(\sqrt{\kappa_-} r) = \kappa_- K_1(\sqrt{\kappa_-} r)$,

we obtain

$$\begin{aligned} &\frac{\beta_2 + \beta_3}{(1 + \beta_2^2) m v} \tilde{\gamma}_- \\ &= \left\{ \left[1 + \frac{\lambda^2 (1 - \beta_2 \beta_3)^2}{\lambda_{\tau}^2 (1 + \beta_2^2)^2} \right] \kappa_- - \frac{1 - \beta_2 \beta_3}{\lambda_{\tau}^2 (1 + \beta_2^2)} \right\} \gamma_-. \end{aligned}$$

Substituting here the root of Eq. (60), we have

$$\tilde{\gamma}_- = \frac{2m\beta_2}{\tau \left[1 + \sqrt{1 - 4 \frac{\lambda^2 \beta_2 (\beta_2 + \beta_3)}{\lambda_{\tau}^2 (1 + \beta_2^2)^2}} \right]} \gamma_- \approx \frac{m\beta_2}{\tau} \gamma_-. \quad (64)$$

Similarly, using the function $K_1(\sqrt{\kappa_+} r)$, from the second equation in Eq. (55), we find

$$\begin{aligned} \gamma_+ &= \frac{2\tau(\beta_2 + \beta_3)\lambda^2}{m(1 + \beta_2^2) \left[1 + \sqrt{1 - 4 \frac{\lambda^2 \beta_2 (\beta_2 + \beta_3)}{\lambda_{\tau}^2 (1 + \beta_2^2)^2}} \right] \lambda_{\tau}^2} \tilde{\gamma}_+ \\ &\approx \frac{\tau(\beta_2 + \beta_3)\lambda^2}{m(1 + \beta_2^2)\lambda_{\tau}^2} \tilde{\gamma}_+ = \frac{\tau_3(\beta_2 + \beta_3)}{m(1 + \beta_3^2)} \tilde{\gamma}_+. \end{aligned} \quad (65)$$

We see that only six of the eight constants introduced above are independent. Indeed, these constants arise from the solutions in Eqs. (62) and (63) of Eq. (56), which were derived from Eqs. (51a) and (51b) by differentiations, which leads to an increase in the number of solutions.

Let us now find a solution to Eq. (52). In radial variables [see the formulas in Eq. (F3) in Appendix F]; they are written in the form:

$$\begin{aligned} \frac{\partial \Pi_{rr}}{\partial r} + \frac{2\Pi_{rr}}{r} + \frac{1}{r} \frac{\partial \Pi_{r\theta}}{\partial \theta} &= \frac{\partial \Phi}{\partial r} + \frac{m}{\tau} \frac{1}{r} \frac{\partial \psi}{\partial \theta}, \\ \frac{\partial \Pi_{r\theta}}{\partial r} + \frac{2\Pi_{r\theta}}{r} - \frac{1}{r} \frac{\partial \Pi_{rr}}{\partial \theta} &= \frac{1}{r} \frac{\partial \Phi}{\partial \theta} - \frac{m}{\tau} \frac{\partial \psi}{\partial r}. \end{aligned} \quad (66)$$

By substituting into them

$$\Phi(\mathbf{r}) = 2\text{Re}\{\varphi(r) \exp(i\theta)\},$$

$$\Pi_{\alpha\beta}(\mathbf{r}) = 2\text{Re}\{Q_{\alpha\beta}(r) \exp(i\theta)\},$$

$$\psi(\mathbf{r}) = 2\text{Re}[\chi \exp(i\theta)],$$

we get

$$\begin{aligned} \frac{\partial Q_{rr}}{\partial r} + \frac{2Q_{rr}}{r} + i \frac{Q_{r\theta}}{r} &= \frac{\partial \varphi}{\partial r} + i \frac{m}{\tau} \frac{\chi}{r}, \\ \frac{\partial Q_{r\theta}}{\partial r} + \frac{2Q_{r\theta}}{r} - i \frac{Q_{rr}}{r} &= i \frac{\varphi}{r} - \frac{m}{\tau} \frac{\partial \chi}{\partial r}, \end{aligned} \quad (67a)$$

or

$$r^2 \frac{\partial^2 Q_{r\theta}}{\partial r^2} + 5r \frac{\partial Q_{r\theta}}{\partial r} + 3Q_{r\theta} = \frac{\partial F}{\partial r},$$

$$\begin{aligned}
 Q_{rr} &= -ir \frac{\partial Q_{r\theta}}{\partial r} - 2iQ_{r\theta} - \varphi - \frac{im}{\tau} r \frac{\partial \chi}{\partial r}, \\
 F(r) &= 2ir\varphi - \frac{m}{\tau} r \frac{\partial(r\chi)}{\partial r}. \quad (67b)
 \end{aligned}$$

The following calculations, due to their cumbersome nature, we place in the Appendix G. As a result, we obtain the closed system of equations for the constants γ_{\pm} , $\tilde{\gamma}_{\pm}$, and the corresponding solutions for ϕ , χ , and Π_{ik} .

C. Resistivity tensor

First, note that, according to the expressions in Eqs. (62), (63), and formulas for κ_{\pm} after Eq. (60), there are two scales of change of physical quantities as functions of the distance from the center of the disk. They are the characteristic lengths related to the eigenvalues of our problem [which are the roots in Eq. (60)]: $1/\sqrt{\kappa_{+}} \approx \lambda$ and $1/\sqrt{\kappa_{-}} \approx \lambda_{\tau}$.

The scale λ_{τ} is always much larger than the disk radius and even the distance between the disks, while λ can be both much smaller and much larger than the disk radius. In the first case, we have a narrow kinetic layer around the disk in which, strictly speaking, we should solve the kinetic equation, while outside this layer, the standard hydrodynamics works, and all spatial dependences are slow. In the second case, the flow also allows a macroscopic description, although not everywhere in terms of standard hydrodynamics.

Substituting into Eqs. (47) and (48) the expressions for the components of the tensor $\Pi_{\alpha\beta}(\mathbf{r})$ [see Appendix G, the expressions in Eq. (G3)], after some calculations, we obtain

$$U_{sd} = \frac{2\pi v m n_D L \varepsilon^2}{eR} [\gamma_{-2} \varepsilon_{-} K_2(\varepsilon_{-}) + \gamma_{+2} \varepsilon_{+} K_2(\varepsilon_{+})], \quad (68)$$

and

$$U_H = \frac{BIW}{en_0c} + \frac{2\pi v m n_D W \varepsilon^2}{eR} [\gamma_{-1} \varepsilon_{-} K_2(\varepsilon_{-}) + \gamma_{+1} \varepsilon_{+} K_2(\varepsilon_{+})], \quad (69)$$

where we introduce the notations $\varepsilon^2 = R^2/v\tau \ll 1$, $\varepsilon_{-} = \sqrt{\kappa_{-}}R \ll 1$, $\varepsilon_{+} = \sqrt{\kappa_{+}}R$, and $\gamma_{\mp 1,2}$, being the real and imaginary parts of the coefficients of γ_{\mp} .

In our calculations, the inequality $\varepsilon_{-} \ll 1$ is always satisfied, so we can assume here with sufficient accuracy that $K_2(\varepsilon_{-}) \approx 2/\varepsilon_{-}^2$, whereas ε_{+} can be any $\varepsilon_{+} \gg 1$ at $\lambda \ll R$ as well as $\varepsilon_{+} \ll 1$ at $\lambda \gg R$. In the first case, despite the exponential smallness $K_2(\varepsilon_{+})$, the second terms in square brackets in the expressions in Eqs. (68) and (69) cannot be neglected, as the coefficients $\gamma_{+1,2}$ are exponentially large. Indeed, it can be seen from Eqs. (G8) and (G9) that they include only combinations of $\gamma_{+} K_p(\varepsilon_{+})$, $p = 0, 1, 2$.

Let us first consider the case of $\lambda \ll R$ in the limit of small magnetic fields. Finding the coefficients γ_{\pm} from Eqs. (E8) and (E9) and substituting them into Eqs. (68) and (69), we obtain

$$\rho_{xx} \approx \frac{8\pi v m n_D}{e^2 n_0 \ln A} - \frac{112\pi v m n_D \lambda^2}{e^2 n_0 \ln^2 A R^2}, \quad (70)$$

$$\Delta\rho_H \equiv \rho_H - \rho_H^0 = \frac{8\pi v m n_D}{e^2 n_0 \ln^2 A} \beta_2 + \frac{16\pi v m n_D \lambda^2}{e^2 n_0 \ln^2 A R^2} (8\beta_2 - \beta_3). \quad (71)$$

In both expressions, the main contribution is given by the first terms that coincide with the hydrodynamic results. As for the second terms, for the diagonal resistivity ρ_{xx} , it is small, while the situation for $\Delta\rho_H$ is more complicated.

The magnitude and sign of the second term in Eq. (71) depend on the relation between the lengths l_2 , l_3 , and R . If all the relaxation lengths are of the same order, the second terms are small compared with the first ones, so that the hydrodynamic corrections dominate. This demonstrates the stability of hydrodynamics, the equations of which were derived under the assumption that $l_2 \ll l_3$ or $l_2 \sim l_3$, and both lengths are smaller than the characteristic space scale of the flow. More interesting is the situation when $l_3 \gg l_2$, which is realized in a degenerate electron Fermi gas [49]. In this case and under the additional condition $l_3 \gg R$, the second term in the right part of Eq. (71) is larger than the first term and has a different sign. Thus, we have

$$\Delta\rho_H \approx -\frac{16\pi v m n_D \lambda^2}{e^2 n_0 \ln^2 A R^2} \beta_3 = -\frac{6\pi v m n_D l_3^2}{e^2 n_0 \ln^2 A R^2} \beta_2. \quad (72)$$

In the case $\lambda \gg R$, the values ρ_{xx} and $\Delta\rho_H$ turn out:

$$\rho_{xx} = \frac{20\pi v m n_D R^2}{e^2 n_0 (26\lambda^2 + 5R^2 \ln A^{1/2})}, \quad (73)$$

$$\Delta\rho_H = -\frac{88\pi v m n_D R^2 \lambda^2}{e^2 n_0 (26\lambda^2 + 5R^2 \ln A^{1/2})^2} \beta_3. \quad (74)$$

At the conditions $R^2 \ll \lambda^2 \ll R^2 \ln A^{1/2}$, the main contributions to Eqs. (70) and (73) coincide, and Eq. (74) differs from Eq. (72) only by a factor close to unity. At $\lambda^2 \gg R^2 \ln(\lambda_{\tau}/R)$, we arrive at the results:

$$\rho_{xx} \approx \frac{10\pi v m n_D R^2}{13e^2 n_0 \lambda^2} = \frac{10\pi m n_D R^2}{13e^2 n_0 \tau_3}, \quad (75)$$

$$\Delta\rho_H \approx -\frac{88\pi v m n_D R^2}{676e^2 n_0 \lambda^2} \beta_3 = -\frac{66\pi R^2 n_D}{169} \rho_H^0. \quad (76)$$

This result is very unexpected. Indeed, the longitudinal resistance does not depend on the relaxation time of the second harmonic of the distribution function, i.e., on the viscous stress relaxation time, and the correction to the Hall resistance does not depend on the relaxation times of both the second and third harmonics but depends only on the size and concentration of disks. This means that, within the three-harmonic approximation, there is a regime that is radically different from the hydrodynamic one. From Eq. (75), we see that $\tau \sim \tau_3/n_D R^2$, whence it follows $\lambda_{\tau} \sim \lambda/\sqrt{n_D R^2} \gg \lambda$.

The expression in Eq. (73) can be interpreted as the resistance of the system of two parallel channels, the hydrodynamic one and the nonhydrodynamic one:

$$\begin{aligned}
 \frac{1}{\rho_{xx}} &= \frac{e^2 n_0 \tau_h}{m} + \frac{e^2 n_0 \tau_{nh}}{m}, \\
 \tau_h &= \frac{\ln A}{2\pi l_2^2 n_D} \tau_2 \gg \tau_2, \\
 \tau_{nh} &= \frac{13}{10\pi n_D R^2} \tau_3 \gg \tau_3.
 \end{aligned}$$

The first term in the right-hand side of this expression coincides with the conductivity in the hydrodynamic regime, and the second term is the conductivity in the nonhydrodynamic

regime discussed above. Introducing notation $\Pi_{ik,h}$ for the hydrodynamic viscosity tensor:

$$\begin{aligned}\Pi_{xx,h} &= -\Pi_{yy,h} = -mv \left(\frac{\partial V_x}{\partial x} - \frac{\partial V_y}{\partial y} \right), \\ \Pi_{xy,h} &= \Pi_{yx,h} = -mv \left(\frac{\partial V_x}{\partial y} + \frac{\partial V_y}{\partial x} \right),\end{aligned}$$

and using Eq. (50), we obtain a diffusionlike equation for dynamics of the shear stress:

$$\frac{1}{\tau_2} \Pi_{ik} = \frac{1}{\tau_2} \Pi_{ik,h} + v_3 \Delta \Pi_{ik}, \quad v_3 = \frac{1}{4} v_F l_3.$$

In the hydrodynamic regime, the first term dominates in the right part of this equation, whereas in the nonhydrodynamic regime, when $R \ll \lambda$, the second term plays the main role in the regions $r < \lambda$. In this case, the balance between relaxation and diffusion of the shear stress tensor is established:

$$-v_3 \Delta \Pi_{ik} = -\frac{1}{\tau_2} \Pi_{ik}.$$

The voltage applied to the sample is approximately equal to the sum of the voltages on the regions $r < \lambda$ and on the internal areas of disk.

We note that the described picture breaks down already in the very small magnetic fields when the inequality $\lambda < R$, equivalent to the inequality:

$$\beta_2 > \frac{l_2}{3R} \sqrt{\frac{\tau_2}{\tau_3}} \ll 1,$$

becomes valid.

It is instructive to compare these results with the results of calculation of the Poiseuille flow in a long sample within the three-harmonic approximation. The last consideration was performed in recent work [46]. For such a flow, the Hall voltage takes the form:

$$eU_H = \frac{B}{n_0 c} I - \Pi_{xx}(W) - \Pi_{xx}(0). \quad (77)$$

In narrow samples $l_2, l_3 \ll W$, this general formula yields

$$\begin{aligned}U_H &= \frac{B}{en_0 c} I - \beta_2 E_x W + \frac{\beta}{1 + \lambda_3/\lambda} E_x W, \\ \lambda_3/\lambda &\sim \frac{1}{\sqrt{1 + \beta_3^2}} \sqrt{\frac{l_3}{l_2}}.\end{aligned} \quad (78)$$

The first two terms on the right-hand side of this expression are the hydrodynamic bulk contribution: the first one is the main part, whereas the second one is the Hall viscosity correction. The third term in Eq. (78) corresponds to the voltage drop in the narrow near-edge layers, with the widths of the order of $\sqrt{l_3 l_2}/(1 + \beta_3^2) \ll W$.

We see that the hydrodynamic correction by its absolute value is always larger than the ballistic correction due to the third harmonic. It is also seen that, at $l_3 \gg l_2$, the hydrodynamic correction dominates, while at $l_3 \approx l_2$, both corrections are of the same order of magnitude and partially compensate each other. It is noteworthy that, for the flow bypassing disks, the situation is the opposite: At $l_3 \gg l_2$, the

third-harmonic ballistic correction may be the main one, while at $l_3 \approx l_2$, it is small as compared with the hydrodynamic one.

In this way, we see that the answer to the question about the magnitude of the correction to the Hall resistance due to the third harmonic is not obvious in advance and depends on the system under study.

Let us briefly discuss the limit $l_3 \rightarrow 0$ (the purely hydrodynamic limit).

In the system with disks in this limit, there, as expected, only the hydrodynamic correction remains, while in the case of the Poiseuille flow, the corrections compensate each other. In other words, for a Poiseuille problem, the result in the limit $l_3 \rightarrow 0$ does not coincide with the formulas we formally put at $l_3 = 0$. It is not difficult to understand how it happens. Indeed, at $l_3 \rightarrow 0$, the width of the edge layers $\sim \sqrt{l_2 l_3}$ tends to zero, while the derivative of velocity and other quantities tends to infinity at $l_3 \rightarrow 0$. Correspondingly, at the edge jumps or boundary layers are formed, where the function $\Pi_{xx}(y)$, whose values at edges determine the Hall voltage by Eq. (78), sharply increases. Thus, all quantities tend to their hydrodynamic values at all points except the very sample edges. Such a singularity is obtained in the framework of the accepted model; however, it is not excluded that considering higher moments in the real problem may somehow cure it.

Finally, let us point out the obvious fact that, if the fourth-harmonic relaxation time τ_4 (or the fourth and higher harmonics relaxation times) is relatively long [for example, $\tau_4 \sim \tau_3$ at the above-discussed case $\tau_2 \ll \tau_3$], then other diverse complex regimes of quasihydrodynamic flows can appear.

IV. COMPARISON WITH EXPERIMENT

A. Qualitative comparison

1. General similarity of experimental data and predictions of theory

Let us compare the theoretical results on longitudinal resistivity obtained in Sec. II with the experimental results of Ref. [27]. As noted in the Introduction, in this paper, a set of high-quality GaAs quantum well samples was fabricated in which localized macroscopic obstacles of various densities were made using electron-beam lithography and subsequent reactive ion etching. Extensive magnetotransport measurements of these samples were performed in Ref. [27], and various types of giant negative magnetoresistance were observed.

In Figs. 3(a)–3(c), we present electron microscope photography of a typical sample studied in experiment [27] and results on the longitudinal resistance in moderate magnetic fields at different temperatures. It is seen that strong negative magnetoresistance with some additional features, depending on temperature, was observed. In Fig. 3(d), we present the result of our calculation of longitudinal resistance in arbitrary units for the samples with rough and smooth disks at two different temperatures. It is seen that the experimental and theoretical curves qualitatively correspond one to another very well.

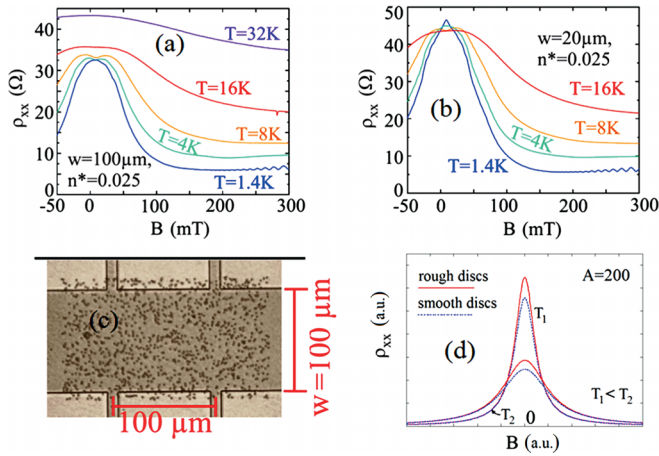


FIG. 3. (a) and (b) Magnetoresistance of GaAs quantum well samples with obstacles fabricated by ion etching at different temperatures T reported in Ref. [27]. Data for samples presented in (a) and (b) differ by their widths w but have the same dimensionless densities of obstacles $n^* = n_D R^2$. The obstacle radius R is $0.42 \mu\text{m}$. (c) Scanning electron microscope photograph of a typical sample. (a)–(c) are taken from Ref. [27]. (d) The results of the developed theory for two different temperatures T_1 and T_2 , $T_2 = 1.5T_1$, for the cases of rough and smooth disks [Eqs. (23) and (27)].

2. Comparison of shapes of experimental and theoretical magnetoresistance

Moreover, we compared the shape of the calculated magnetoresistance curves for the samples with rough and smooth disks studied theoretically with the shape of the experimental magnetoresistance curve corresponding to the lowest temperature (see Fig. 4). It is seen that the calculation result for the disks with smooth edges, from which the electrons were reflected mirrorlike, agrees with the experimental curve much better than the calculation result for the disks with rough edges, which scatter electrons diffusely. The theoretical curve for the latter case in the region of small magnetic fields is

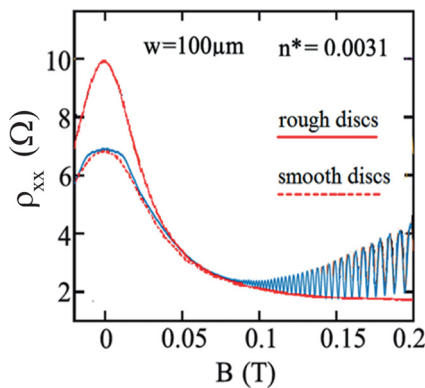


FIG. 4. Magnetoresistance of a GaAs quantum well sample studied in Ref. [27] with obstacles made by ion etching at temperatures $T = 80 \text{ mK}$. Experimental blue curve is taken from Ref. [27]. Solid and dashed red curves are the results of our hydrodynamic theory for the samples with rough and smooth disks. The last curves are plotted by Eqs. (23) and (27), respectively.

sharper than both the experimental and theoretical curves for the smooth disks.

Note that we use arbitrary units in Fig. 4 for the resistance as, in the current subsection, we perform only a qualitative comparison of the experimental data with our predictions.

Based on the results of Fig. 4, we conclude that a detailed comparison of theory and experiment allows us to choose a realistic model of samples with macroscopic obstacles.

B. Quantitative comparison

1. Half-width of magnetoresistance curves

Let us qualitatively discuss the magnetoresistance curves for the two samples studied in Ref. [27] for some intermediate temperature, for example, for 8 K [see Fig. 3(b)].

To characterize the width of magnetoresistance curves, we introduce their half-width $B_{1/2}$. Within the hydrodynamic theory [17,49], this value is determined by the relaxation time of the shear stress τ_2 from the condition $\omega_c(B_{1/2})\tau_2 = 1$. In all samples studied in Ref. [27], the radii of the disks are $R = 0.5 \mu\text{m}$. For sample 1, in which the density of defects is $n_D = 1.24 \times 10^6 \text{ cm}^{-2}$ [the corresponding mean distance between defects is $d = (n_D)^{-1/2} = 9.0 \mu\text{m}$], we obtain for the relaxation length the result $l_2 = v_F \tau_2 = 1.5 \mu\text{m}$ from the value $B_{1/2}$ extracted from the magnetoresistance width. For sample 2, in which the defect density is $n_D = 1.0 \times 10^7 \text{ cm}^{-2}$ [in this sample, we have $d = (n_D)^{-1/2} = 3.2 \mu\text{m}$], we deduce within the same procedure $l_2 = v_F \tau_2 = 1.1 \mu\text{m}$.

Our analysis shows that the mean free path lengths l_2 are smaller than the mean distances between the defects in both samples, as the inequality $d > l_2$ is fulfilled. Thus, a large hydrodynamic contribution to the flow is expected in both samples.

We emphasize that the parameter $B_{1/2}$ is the only fitting parameter in our analysis of experimental data on giant negative magnetoresistance. It yields the value τ_2 , which in turn leads the hydrodynamic contribution to the resistance at zero magnetic field $\Delta\rho(B=0)$. Below, we compare the values $\Delta\rho(B=0)$ calculated for both samples with $n_D = 1.24 \times 10^6$ and $10 \times 10^6 \text{ cm}^{-2}$ with the experimental data on the values $\Delta\rho(B=0)$ in these two samples.

2. Important characteristic magnetic fields

The important characteristic values of the magnetic field are the magnetic field B_R , at which the cyclotron radius takes the value equal to the defect radius, and the field B_d , at which the cyclotron radius turns out to be of the order of the distance between the defects d . For both samples, the field B_R is the same, being equal to 164 mT , and the field B_d is equal to 9.2 mT for sample 1 and 26.0 mT for sample 2. Both fields are shown by vertical lines in Fig. 5.

The physical nature of the regimes determined by these fields are as follows. At $B < B_d$, when $R_c > d$, the ballistic effects are important, related to scatterings of electrons only on disks, without a substantial role of the interparticle scattering. In the diapason $B_d < B < B_R$, corresponding to the inequality $R < R_c < d$, viscous flows are formed in the regions between disks, at distances greater than R_c from disk edges. When $B > B_R$, one should expect a well-formed

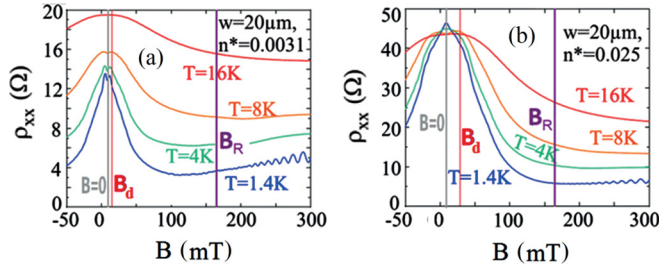


FIG. 5. (a) and (b) From Fig. 4 with added vertical lines corresponding to the characteristic magnetic fields B_R and B_d . Vertical gray line depicts the center of the magnetoresistance curve corresponding to zero magnetic field inside the sample (the scale on horizontal axis, apparently, has an artificial shift).

viscous flow everywhere between disks and with some hydrodynamic boundary conditions at the disk edges. The last ones are formed in the semiballistic layers around disk edges with the width of the order R_c .

3. Amplitude of magnetoresistance

Now we compare the theoretical and experimental values of the relative amplitudes of magnetoresistance, which is the difference of the resistance at $B = 0$ and in the limit $B \gg B_{1/2}$.

For sample 1 with the defect density $n_D = 1.24 \times 10^6 \text{ cm}^{-2}$ (which corresponds to $d/R = 18$), the magnetoresistance amplitude is $\Delta\rho_{\text{exp}}(B=0) \sim 7 \text{ Ohm}$ [see Fig. 6(a)], while the calculation by Eqs. (23) and (27) with the obtained above relaxation time τ_2 yields $\Delta\rho_{\text{theor}}(B=0) = 9.6 \text{ Ohm}$. For sample 2, in which $n_D = 1.0 \times 10^7 \text{ cm}^{-2}$ (this value corresponds to $d/R = 6$), we have $\Delta\rho_{\text{exp}}(B=0) \sim 35 \text{ Ohm}$ [see Fig. 6(b)], while Eqs. (23) and (27) without the logarithm factor $\ln(A)$, which is of the order of unity in this case, yield $\Delta\rho_{\text{theor}}(B=0) \sim 35 \text{ Ohm}$ (recall that our calculations assumed the inequality of $\ln(A) \gg 1$).

We see that the theoretical values of the hydrodynamic contribution to the resistance at zero magnetic field $\Delta\rho(B=0)$, calculated with the time τ_2 obtained from the widths of the magnetoresistance curves, are in reasonable agreement with the experimental values. For the discussed two samples, both values d and R correspond to the not-too-large or even not large (~ 1) parameter $A = (8\pi n_D R^2)^{-1}$ from Eq. (22), by the logarithm of which $\ln(A)$ the decomposition of the solution for the flow was performed. Namely, for sample 1, we have $A = 12.8$ and $\ln(A) = 2.6$. As a result, good agreement be-

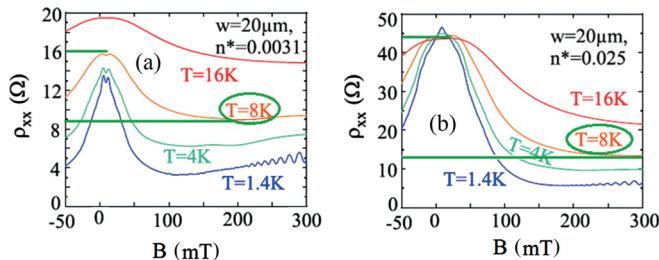


FIG. 6. (a) and (b) From Fig. 4 with added horizontal lines corresponding to the relative height of the magnetoresistance curves at 8 K.

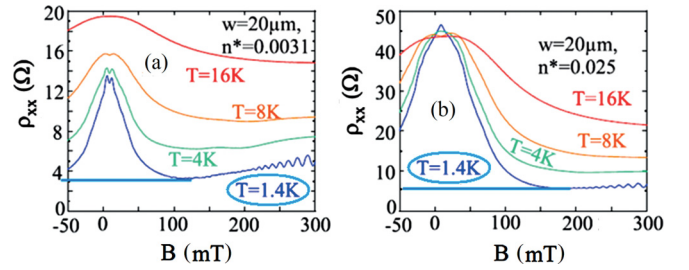


FIG. 7. (a) and (b) From Fig. 4 with added horizontal line corresponding to the resistance in the limit $B \gg B_R$ at lowest temperature 1.4 K.

tween the theoretical and experimental values of $\Delta\rho_{\text{theor}}(B)$ is reached. For sample 2, this value turns out to be $A = 1.5$, and thus, $\ln(A) = 0.47$. Thus, in the last case, the developed theory is applicable only on a qualitative but not quantitative level; the values $\Delta\rho_{\text{theor}}(B=0)$ and $\Delta\rho_{\text{exp}}(B=0)$ are of the same order of magnitude but are numerically different.

4. Residual ohmic resistance

In the limit of very low temperatures, when the interparticle scattering time $\tau_{ee} \sim 1/T^2$ becomes very long, the giant negative magnetoresistance persists (see Fig. 3). The reason for this fact can be in the scattering of electrons on disorder (for example, short-range defects) between the macroscopic defects (disks). Such scattering leads to relaxation of the shear stress with the rate $1/\tau_{2,\text{dis}}$ as well as to some residual momentum relaxation with the rate $1/\tau_{1,\text{dis}}$, leading to the residual resistance. The last value exhibits itself by the longitudinal resistivity $\rho_{xx}(B)$ in the limit $\omega_c \tau_{2,\text{dis}} \gg 1$ [17,50].

Now we perform a quantitative analysis of experimental data for the case of the lowest temperature $T = 1.4 \text{ K}$ (see Fig. 7). From the half-width of the curve $\rho_{xx}(B)$, we extract the time $\tau_{2,\text{dis}}$ by the procedure described above. From the value ρ_{xx} in the limit $\omega_c \tau_{2,\text{dis}} \gg 1$ and the Drude formula $\rho_{xx} = m/(e^2 n_0 \tau_{1,\text{dis}})$, we obtain the experimental value of the transport time $\tau_{1,\text{dis}}$. The resulting times $\tau_{1,\text{dis}}$ and $\tau_{2,\text{dis}}$ differ from one another anomalously strongly. For sample 1, we have $\tau_{1,\text{dis}}/\tau_{2,\text{dis}} = 45$, and for sample 2, we have $\tau_{1,\text{dis}}/\tau_{2,\text{dis}} = 32$. A similar very strong difference of $\tau_{1,\text{dis}}$ and $\tau_{2,\text{dis}}$ was also found when analyzing experimental data obtained on similar samples (see, for example, Refs. [14,17,50]).

Ordinarily, the values of times $\tau_{1,\text{dis}}$, $\tau_{2,\text{dis}}$, $\tau_{3,\text{dis}}$, etc., have the same order of magnitude. A possible reason for the anomalously large difference between $\tau_{1,\text{dis}}$ and $\tau_{2,\text{dis}}$ may be related to the following mechanism. It was proposed in Ref. [52] that dynamically connected pairs of electrons, which repeatedly collide with one another due to their returns induced by the action of the magnetic field, play an important role in transport of 2D electrons at classical magnetic fields. Dynamics of such pairs induced the memory effects in ac hydrodynamic magnetotransport, particularly the magnetooscillations of photoconductivity; those may be a mechanism of the well-known MIRO effect in high-quality samples. It is noteworthy that similar memory effects in magnetotransport, induced by the analog of such extended collisions, have been previously studied for the case of noninteracting electrons in disordered

samples with localized defects (see, for example, Ref. [51] and references therein).

For a rigorous description of the effects associated with such extended collisions, leading to a sharp increase in the degree of correlation of the dynamics of electrons, the Boltzmann equation for the one-particle distribution function of electrons is not sufficient. Possibly, it is necessary to solve the equation not only for the evolution of such distribution function but also for the evolution of spatially inhomogeneous two-particle correlators of electron distributions. For example, the construction of such equations was carried out in Ref. [53] (and in other works by the authors) for the Boltzmann gas of uncharged particles and in Ref. [54] for a degenerated gas of electrons. We are currently studying these correlation effects in relation to our problem for a proper explanation of the giant magnetoresistance of high-quality samples in the limit $T \rightarrow 0$.

V. CONCLUSIONS

We have theoretically studied the magnetotransport of electrons in samples with macroscopic defects (disks) in both the hydrodynamic and quasihydrodynamic regimes. The latter assumes that the third-order harmonics of the electron distribution function as well as the first and second ones, control the flow, in contrast to the hydrodynamic regime, which is based on the approximation of two harmonics.

We have shown that, in the hydrodynamic regime, the resistivity tensor does not depend on the Hall viscosity if the boundary conditions on the obstacles do not depend on it and that the flux profile is independent of the magnetic field if the boundary conditions do not depend on it. We have examined both cases of rough and smooth disk boundaries and have shown that, in both cases, there is strong negative magnetoresistance described by the same expression, up to small corrections. As for the Hall resistivity, in the case of rough boundaries of the disks, it is exactly equal to the standard value B/en_0c because the boundary conditions in this case do not depend on the magnetic field and the Hall viscosity. In the case of smooth boundaries, there is a small correction to the standard value proportional to the Hall viscosity (the boundary conditions depend on the Hall viscosity and the magnetic field).

Based on the obtained results, we argue that the correction to the standard value of the Hall resistivity is an important characteristic of the type of defect edge. Namely, the smoother the disk edges, the larger the deviation of the Hall resistance from its standard value. Moreover, the dependence of the correction in the Hall resistance on the magnetic field provides information about the relationship between the relaxation times of the second and higher harmonics of the distribution function. However, more precise experiments than Refs. [13,27] are needed for this purpose.

In the second part of the paper, we derive quasihydrodynamic equations from the kinetic equation based on the three-harmonic approximation for the distribution function and solve them for the case of smooth disks. It is shown that, depending on the relation between the relaxation lengths l_2 , l_3 and the disk radius R , the expression for the resistivity tensor may coincide with the hydrodynamic one or may differ from it. We assume that, throughout the paper, the inequality

$l_2 \ll R$ is fulfilled, whereas l_3 can be any length. At $l_3 \ll R$, the resistivity tensor coincides with the hydrodynamic one, regardless of the relation between l_2 and l_3 . In other words, our calculations show that hydrodynamics works not only under the condition $l_3 \ll l_2$, which is usually taken when deriving the equations of hydrodynamics from the kinetic equation, but also under any relation between l_3 and l_2 , if $\sqrt{l_3 l_2} \ll R$ and $l_3 \ll R$. If $\sqrt{l_3 l_2} \ll R$ and $l_3 \gg R$, the longitudinal resistivity remains hydrodynamic, while the correction to the standard Hall resistivity becomes nonhydrodynamic. Under the condition $\sqrt{l_3 l_2} \gg R$, the situation is different. At a sufficiently large value of $\sqrt{l_3 l_2}$ (the exact inequality is given in the main text of the paper), the flow regime that is far from the hydrodynamic one is realized. In this regime, the longitudinal resistivity is independent of l_2 , and the correction $\delta\rho_H$ to the standard the Hall resistivity $\rho_H^0 = B/n_0ec$ is independent of both lengths l_3 and l_2 but depends only on the radius and concentration n_D of the disks $\delta\rho_H \sim n_D R^2 \rho_H^0$.

We have compared the obtained theoretical results with experiment [27] on the magnetotransport of GaAs quantum well samples with artificially made localized defects of different densities. Good qualitative agreement between the theoretical and experimental magnetoresistance curves is demonstrated. The analysis shows that the model of smooth disks with a relatively high density of disks describes the experimental data better than the model of rough disks. We have also performed a quantitative analysis of the experimental data on the parameters of magnetoresistance curves for two samples with different densities of defects.

We consider that our results will be useful in analyzing and interpreting experiments on hydrodynamic transport in samples with 2D viscous electron fluid and macroscopic localized defects. We hope that the type of giant negative magnetoresistance, which in Ref. [24] is called *bell-shaped magnetoresistance*, is explained by our mechanism. This is supported by the absence of experimental dependence of the magnetoresistance on the width of the sample and the temperature dependence typical for the magnetoresistance related to the diagonal viscosity (see discussion in Ref. [17]).

Based on the obtained results, we also argue that the correction to the standard value of the Hall resistivity is an important characteristic of the type of defect edge. Namely, the smoother the disk edges, the larger the deviation of the Hall resistance from its standard value. Moreover, the dependence of the correction in the Hall resistance on the magnetic field provides information about the relationship between the relaxation times of the second and higher harmonics of the distribution function.

ACKNOWLEDGMENTS

We thank I. V. Gornyi and D. G. Polyakov, who took an active part in the discussions throughout the work on the problem. They plan to publish an article soon devoted to the same problem but considered in a slightly different approach. In their work, some other aspects of the problem are planned to be considered with closer attention.

This work was supported by the Russian Science Foundation (Grant No. 22-12-00139).

APPENDIX A: EXPRESSIONS FOR HYDRODYNAMIC VELOCITIES AVERAGED OVER FLOW REGION

In this section, we demonstrate how the terms with sample-averaged velocities \bar{V}_x and \bar{V}_y arise in Eq. (8). For example, the transfer of the function $-m\omega_c\psi/e$ to the right-hand side of Eq. (6) in the first equation gives

$$\frac{m\omega_c}{eS} \int_0^W [\psi(L, y) - \psi(0, y)] dy.$$

Let us now calculate the sample average velocity:

$$\begin{aligned} \frac{m\omega_c}{e} \bar{V}_y &= \frac{m\omega_c}{eS} \int_0^W dy \int_0^L dx V_y(x, y) \\ &= \frac{m\omega_c}{eS} \int_0^W dy \int_0^L dx \frac{\partial \psi(x, y)}{\partial x} \\ &= \frac{Rm\omega_c}{eS} \sum_k \oint_{\Gamma_k} \psi \cos \theta_k d\theta_k \\ &\quad + \frac{m\omega_c}{eS} \int_0^W [\psi(L, y) - \psi(0, y)] dy. \end{aligned} \quad (\text{A1})$$

Here, the second term in the right part coincides with the above expression arising from the transfer of the function $-m\omega_c\psi/e$ to the right part of Eq. (6), while the first term is zero because, at the edges of the disks, $\psi = \text{const.}$ due to the condition $V_r = \partial\psi/r\partial\theta = 0$.

In this way, Eq. (A1) connects the mean velocity \bar{V}_y with the expressions containing the function ψ along the sample and the disk edges.

APPENDIX B: GENERALIZATION OF THE THEOREM ABOUT ABSENCE OF DEPENDENCE OF RESISTIVITY TENSOR ON HALL VISCOSITY

Here, we consider a sample with macroscopic defects of any form. We will show that properties of the electron fluid

are also independent of the Hall viscosity if the defects edges are rough. Thus, the corresponding theorem formulated in Sec. II A has a general character.

In the case of an arbitrarily shaped obstacle, instead of Eq. (9), we will have the equations:

$$\begin{aligned} -m\omega_c \bar{V}_y - \frac{eU_{sd}}{L} - \frac{R}{S} \sum_k \oint_{\Gamma_k} \tilde{\Psi} dy - \frac{mvR}{eS} \sum_k \oint_{\Gamma_k} \Omega dx &= 0, \\ m\omega_c \bar{V}_x - \frac{eU_H}{W} + \frac{R}{S} \sum_k \oint_{\Gamma_k} \tilde{\Psi} dx - \frac{mvR}{S} \sum_k \oint_{\Gamma_k} \Omega dy &= 0. \end{aligned} \quad (\text{B1})$$

From Eq. (5), it follows that Ω does not depend on the Hall viscosity, and from Eq. (4), it follows that the flow function can be presented in the form:

$$\tilde{\Psi} = \tilde{\Psi}_1 + \tilde{\Psi}_2,$$

where $\tilde{\Psi}_1(x, y)$ does not depend on ν_H , but $\tilde{\Psi}_2$ does not depend on the coordinates. Since $\int_{\Gamma_k} \text{const.}(x, y) dx = \int_{\Gamma_k} \text{const.}(x, y) dy = 0$, it immediately follows from Eq. (B1) that the voltages U_{sd} and U_H , and thus the components of the resistivity tensor, are independent of the Hall viscosity. The independence of the velocity profile in the sample with such boundary conditions on the magnetic field follows from Eq. (5).

APPENDIX C: CALCULATION OF WORK OF THE HALL VISCOSITY TERM IN THE NAVIER-STOKES EQUATION

Below, we calculate the work from the force originated from the Hall viscosity term and show that it is equal to zero:

$$\begin{aligned} A_H &= \frac{mv_H}{e} \int [\Delta \mathbf{V} \times \mathbf{e}_z] \mathbf{V} d^2 \mathbf{r} = \frac{mv_H}{e} \int (V_x \Delta V_y - V_y \Delta V_x) d^2 \mathbf{r} = \frac{mv_H}{e} \int \text{div}(V_x \nabla V_y - V_y \nabla V_x) d^2 \mathbf{r} \\ &= -\frac{mv_H R}{e} \sum_k \oint_{\Gamma_k} \left(V_x \frac{\partial V_y}{\partial r} - V_y \frac{\partial V_x}{\partial r} \right) d\theta = (V_r = 0) \\ &= \frac{mv_H R}{e} \sum_k \oint_{\Gamma_k} \left[(V_r \cos \theta - V_\theta \sin \theta) \frac{\partial (V_r \sin \theta + V_\theta \cos \theta)}{\partial r} - (V_r \sin \theta + V_\theta \cos \theta) \frac{\partial (V_r \cos \theta - V_\theta \sin \theta)}{\partial r} \right] d\theta \\ &= -\frac{mv_H R}{e} \sum_k \oint_{\Gamma_k} V_\theta \frac{\partial V_r}{\partial r} d\theta = \left(V_\theta = \frac{\partial \psi}{\partial r}, V_r = -\frac{1}{r} \frac{\partial \psi}{\partial \theta} \right) = \frac{mv_H R}{e} \sum_k \oint_{\Gamma_k} \frac{\partial \psi}{\partial r} \frac{\partial}{\partial r} \left(\frac{1}{r} \frac{\partial \psi}{\partial \theta} \right) d\theta \\ &= -\frac{mv_H}{eR} \sum_k \oint_{\Gamma_k} \frac{\partial \psi}{\partial r} \frac{\partial \psi}{\partial \theta} d\theta + \frac{mv_H}{e} \sum_k \oint_{\Gamma_k} \frac{\partial \psi}{\partial r} \frac{\partial^2 \psi}{\partial \theta \partial r} d\theta = 0 + \frac{mv_H}{2e} \sum_k \oint_{\Gamma_k} \frac{\partial}{\partial \theta} \left(\frac{\partial \psi}{\partial r} \right)^2 d\theta = 0 + 0 = 0. \end{aligned}$$

APPENDIX D: DERIVATION OF THE EFFECTIVE MEDIUM EQUATION

In this section, we provide a detailed derivation of Eq. (10) for the case of the absence of a magnetic field (in the presence of a magnetic field, the calculations are similar but more

cumbersome and contain nothing ideologically new). For this purpose, let us introduce the function:

$$H(\mathbf{r}; \mathbf{r}_1, \dots, \mathbf{r}_N) = 1 - \sum_{j=1}^N h(R - |\mathbf{r} - \mathbf{r}_j|), \quad (\text{D1})$$

where $h(x)$ is the stepped Heaviside function, and the points \mathbf{r}_j describe the positions of the centers of the disks. In addition, we introduce the probability density of the given disk configuration $P(\mathbf{r}_1, \dots, \mathbf{r}_N)$, so that the mean value of the value $Q(\mathbf{r}; \mathbf{r}_1, \dots, \mathbf{r}_N)$ at a point \mathbf{r} is given by an integral:

$$\langle Q \rangle(\mathbf{r}) = \int Q(\mathbf{r}; \mathbf{r}_1, \dots, \mathbf{r}_N) P(\mathbf{r}_1, \dots, \mathbf{r}_N) d\mathbf{r}_1 \cdots d\mathbf{r}_N.$$

In the following, we will assume the distribution of disks to be random and, on average, homogeneous. Disks cannot overlap, so in general, $P(\mathbf{r}_1, \dots, \mathbf{r}_N) = 0$ at $|\mathbf{r}_i - \mathbf{r}_j| < 2R$. We will not consider this restriction since it leads to quadratic corrections in the small parameter $R^2 n_D$. This means that $P(\mathbf{r}_1, \dots, \mathbf{r}_N) = p(\mathbf{r}_1) \cdots p(\mathbf{r}_N)$, where $p(\mathbf{r}_i) = 1/S$. Multiplying the x component of Eq. (1) by the function H and averaging the result over the positions of all disks gives

$$e\langle HE_x \rangle = mv \operatorname{div} \langle (H \nabla V_x) \rangle - mv \langle \nabla V_x \cdot \nabla H \rangle. \quad (\text{D2})$$

It is not difficult to show (see, e.g., Ref. [39]) that $\operatorname{div} \langle (H \nabla V_x) \rangle = \Delta \langle V_x \rangle$. In the case of a homogeneous disk distribution, $\Delta \langle V_x \rangle = 0$. Taking advantage of the symmetry of the integrand with respect to the permutations of disks, we obtain from Eqs. (D1) and (D2)

$$e\langle HE_x \rangle = -mv n_D \int \delta(R - |\mathbf{r} - \mathbf{r}_1|) \nabla \langle V_x \rangle_1 \cdot \mathbf{e}_1 d\mathbf{r}_1, \quad (\text{D3})$$

$$\mathbf{e}_1 = \frac{\mathbf{r} - \mathbf{r}_1}{|\mathbf{r} - \mathbf{r}_1|},$$

where $\langle V_x \rangle_1$ is the average, assuming one disk is fixed:

$$\langle V_x \rangle_1 = \int V_x(\mathbf{r}; \mathbf{r}_1, \dots, \mathbf{r}_N) \frac{d\mathbf{r}_2 \cdots d\mathbf{r}_N}{S^{N-1}}.$$

It is clear that $\langle V_x \rangle_1$ is a function of the difference $\mathbf{r} - \mathbf{r}_1$, which allows us to go from integration over \mathbf{r}_1 in Eq. (D3) to integration over $\rho = \mathbf{r} - \mathbf{r}_1$. Considering the δ function, we obtain

$$e\langle HE_x \rangle = mv n_D R \int \frac{\partial \langle V_x \rangle_1}{\partial \rho} d\theta. \quad (\text{D4a})$$

It comes out in the same way:

$$e\langle HE_y \rangle = mv n_D R \int \frac{\partial \langle V_y \rangle_1}{\partial \rho} d\theta. \quad (\text{D4b})$$

Now using the relations in Eq. (2), we find

$$e\langle HE_x \rangle = mv R n_D \oint_{\Gamma} \langle \Omega \rangle_1 \sin \theta d\theta, \quad (\text{D5})$$

$$e\langle HE_y \rangle = -mv R n_D \oint_{\Gamma} \langle \Omega \rangle_1 \cos \theta d\theta.$$

These equalities do not consider the field inside the disks. For this field, we have

$$e\langle (1 - H)E_x \rangle = -en_D \int h(R - \rho) \langle E_x \rangle_1 d\rho,$$

$$e\langle (1 - H)E_y \rangle = -en_D \int h(R - \rho) \langle E_y \rangle_1 d\rho,$$

which by virtue of Eq. (4) can be written in the form:

$$e\langle (1 - H)E_x \rangle = mv n_D \int h(R - \rho) \frac{\partial \langle \Omega \rangle_1}{\partial y} d\rho,$$

$$e\langle (1 - H)E_y \rangle = -mv n_D \int h(R - \rho) \frac{\partial \langle \Omega \rangle_1}{\partial x} d\rho,$$

or after simple transformations, in the form:

$$e\langle (1 - H)E_x \rangle = -mv R n_D \int_{\Gamma} R \frac{\partial \langle \Omega \rangle_1}{\partial \rho} \sin \theta d\theta,$$

$$e\langle (1 - H)E_y \rangle = mv R n_D \int_{\Gamma} R \frac{\partial \langle \Omega \rangle_1}{\partial \rho} \cos \theta d\theta. \quad (\text{D6})$$

Adding Eqs. (D5) and (D6) and considering that $\langle E_x \rangle = -U_x/L$ and $\langle E_y \rangle = -U_y/L$, for $B \neq 0$, we obtain Eq. (10).

From symmetry considerations, it follows that the integrals in the right parts of Eq. (D4), and hence in the right parts of Eqs. (15) and (16), are proportional to the mean flow velocity ($\bar{V}_x = \langle V_x \rangle$, $\bar{V}_y = \langle V_y \rangle$), so that the right parts of Eq. (10) take the form:

$$mv R n_D \oint_{\Gamma} \left(R \frac{\partial \langle \Omega \rangle_1}{\partial r} - \langle \Omega \rangle_1 \right) \sin \theta d\theta = \frac{m \bar{V}_x}{\tau} + m \delta \omega_c \bar{V}_y,$$

$$-mv R n_D \oint_{\Gamma} \left(R \frac{\partial \langle \Omega \rangle_1}{\partial r} - \langle \Omega \rangle_1 \right) \cos \theta d\theta = \frac{m \bar{V}_x}{\tau} - m \delta \omega_c \bar{V}_x. \quad (\text{D7})$$

Here, the relaxation time τ and the shift of the cyclotron frequency $\delta \omega_c$ are to be determined.

Now we need to derive equations for the values $\langle \mathbf{V} \rangle_1$, $\langle \mathbf{E} \rangle_1$, and $\langle \Omega \rangle_1$. For this purpose, we fix one of the disks and, multiplying Eq. (1) by H , we average it over the positions of the other disks. Then for the average local field in the flow region, we obtain (again, we temporarily assume that $B = 0$):

$$e\langle HE_x \rangle_1 = mv \Delta \langle V_x \rangle_1 - mv n_D \int \delta(R - |\mathbf{r} - \mathbf{r}_2|) \times \nabla \langle V_x \rangle_{1,2} \cdot \mathbf{e}_2 d\mathbf{r}_2,$$

$$e\langle HE_y \rangle_1 = mv \Delta \langle V_y \rangle_1 - mv n_D \int \delta(R - |\mathbf{r} - \mathbf{r}_2|) \times \nabla \langle V_y \rangle_{1,2} \cdot \mathbf{e}_2 d\mathbf{r}_2,$$

where $\langle Q \rangle_{1,2}$ is the average provided that the positions of the two disks are fixed:

$$\langle Q \rangle_{1,2} = \int Q(\mathbf{r}, \mathbf{r}_1, \mathbf{r}_2; \mathbf{r}_3, \dots, \mathbf{r}_N) \frac{d\mathbf{r}_3 \cdots d\mathbf{r}_N}{S^{N-2}}.$$

For the field in the area occupied by disks, we obtain, like Eq. (D6),

$$e\langle (1 - H)E_x \rangle_1 = n_D \int h(R - |\mathbf{r} - \mathbf{r}_2|) \langle E_x \rangle_{1,2} d\mathbf{r}_2,$$

and for the mean total field, we will have ($B \neq 0$)

$$e\langle E_x \rangle_1 = mv \Delta \langle V_x \rangle_1 - m \omega_c \langle V_y \rangle_1 - mv R n_D \oint_{\Gamma} \left(R \frac{\partial \langle \Omega \rangle_{12}}{\partial r} - \langle \Omega \rangle_{12} \right) \sin \theta d\theta,$$

$$e\langle E_y \rangle_1 = mv \Delta \langle V_y \rangle_1 + m \omega_c \langle V_x \rangle_1 + mv R n_D \oint_{\Gamma} \left(R \frac{\partial \langle \Omega \rangle_{12}}{\partial r} - \langle \Omega \rangle_{12} \right) \cos \theta d\theta.$$

Finally, assuming, following Ref. [39], that the integrals in these equations are expressed over $\langle V_x \rangle_1$ and $\langle V_y \rangle_1$ in the same

way as the analogous integrals in Eq. (D7) are expressed over \vec{V}_x and \vec{V}_y , we obtain Eq. (11) (in it, the angle brackets and the subscript 1 for the velocity and electric field vectors are omitted). The point of the assumptions made is the idea of

imagining the second disk, located in the R neighborhood of the point \mathbf{r} , being in a stream flowing at a large distance from it with velocity $\langle \mathbf{V} \rangle_1(\mathbf{r} - \mathbf{r}_1)$ rather than $\langle \mathbf{V} \rangle$. In Ref. [39], the corresponding calculations are presented.

APPENDIX E: SYSTEM OF EQUATIONS FOR THE DISTRIBUTION FUNCTION IN THE THREE-HARMONIC APPROXIMATION

In this section, we present the detailed equations for the amplitudes of the angular harmonics of the truncated distribution function, which follow from the kinetic equation.

Substituting the expression in Eq. (49) into the kinetic equation, we obtain a system of equations:

$$\begin{aligned}
\frac{v}{2} \frac{\partial f_{2c}}{\partial x} + \frac{v}{2} \frac{\partial f_{2s}}{\partial y} - eE_x v f'_F + \omega_c f_{1s} &= 0, \\
-\frac{v}{2} \frac{\partial f_{2c}}{\partial y} + \frac{v}{2} \frac{\partial f_{2s}}{\partial x} - eE_y v f'_F - \omega_c f_{1c} &= 0, \quad \frac{\partial f_{1c}}{\partial x} + \frac{\partial f_{1s}}{\partial y} = 0, \\
\frac{v}{2} \left(\frac{\partial f_{1c}}{\partial x} - \frac{\partial f_{1s}}{\partial y} + \frac{\partial f_{3c}}{\partial x} + \frac{\partial f_{3s}}{\partial y} \right) + 2\omega_c f_{2s} + \frac{1}{\tau_2} f_{2c} &= 0, \\
\frac{v}{2} \left(\frac{\partial f_{1c}}{\partial y} + \frac{\partial f_{1s}}{\partial x} - \frac{\partial f_{3c}}{\partial y} + \frac{\partial f_{3s}}{\partial x} \right) - 2\omega_c f_{2c} + \frac{1}{\tau_2} f_{2s} &= 0, \\
f_{3c} &= \frac{l_3}{2(1 + \beta_3^2)} \left(-\frac{\partial f_{2c}}{\partial x} + \frac{\partial f_{2s}}{\partial y} + \beta_3 \frac{\partial f_{2c}}{\partial y} + \beta_3 \frac{\partial f_{2s}}{\partial x} \right), \\
f_{3s} &= -\frac{l_3}{2(1 + \beta_3^2)} \left(\frac{\partial f_{2s}}{\partial x} + \frac{\partial f_{2c}}{\partial y} + \beta_3 \frac{\partial f_{2c}}{\partial x} - \beta_3 \frac{\partial f_{2s}}{\partial y} \right). \quad (E1)
\end{aligned}$$

We can exclude the third-order harmonics f_{3s} and f_{3c} from these equations:

$$\begin{aligned}
\frac{l_2}{2} \frac{\partial f_{1c}}{\partial x} - \frac{l_2}{2} \frac{\partial f_{1s}}{\partial y} - \frac{l_2 l_3}{4(1 + \beta_3^2)} (\Delta f_{2c} - \beta_3 \Delta f_{2s}) + \beta f_{2s} + f_{2c} &= 0, \quad \beta_3 = 3\omega_c \tau_3, \quad l_n = v \tau_n, \\
\frac{l_2}{2} \frac{\partial f_{1c}}{\partial y} + \frac{l_2}{2} \frac{\partial f_{1s}}{\partial x} - \frac{l_2 l_3}{4(1 + \beta_3^2)} (\Delta f_{2s} + \beta_3 \Delta f_{2c}) - \beta f_{2c} + f_{2s} &= 0. \quad (E2)
\end{aligned}$$

Note that, according to our condition of instantaneous relaxation of all harmonics beginning with the fourth harmonic, in the expressions for f_{2c} and f_{2s} , there is no contribution of the fourth harmonic.

According to the definitions in Eq. (37), we have

$$\begin{aligned}
\Pi_{xx} = -\Pi_{yy} &= \frac{\pi m}{n_0} \int f_{2c} v^2 \frac{pdp}{(2\pi \hbar)^2}, \quad \Pi_{xy} = \Pi_{yx} = \frac{\pi m}{n_0} \int f_{2s} v^2 \frac{pdp}{(2\pi \hbar)^2}, \\
V_x &= \frac{2\pi}{n_0} \int f_{1c} v \frac{pdp}{(2\pi \hbar)^2}, \quad V_y = \frac{2\pi}{n_0} \int f_{1s} v \frac{pdp}{(2\pi \hbar)^2}. \quad (E3)
\end{aligned}$$

Multiplying Eq. (E2) by v_i and $v_i v_k$ and integrating, we obtain Eq. (50).

APPENDIX F: BOUNDARY CONDITIONS AT EDGES OF SMOOTH DISKS

Here, we derive the boundary conditions at the disk edges for the momentum flux tensor calculated on the truncated three-harmonic distribution function.

The condition in Eq. (57) on the distribution function can be rewritten as

$$\begin{aligned}
[1 - (-1)^n \cos 2n\theta] f_{nc} - (-1)^n \sin 2n\theta f_{ns} &= 0, \\
-(-1)^n \sin 2n\theta f_{nc} + [1 + (-1)^n \cos 2n\theta] f_{ns} &= 0. \quad (F1)
\end{aligned}$$

These equations connect the functions $f_{nc}(\varepsilon, R, \theta)$ and $f_{ns}(\varepsilon, R, \theta)$:

$$f_{nc} \sin n\theta = f_{ns} \cos n\theta, \quad n = 2k; \quad f_{nc} \cos n\theta = -f_{ns} \sin n\theta, \quad n = 2k + 1. \quad (F2)$$

For $n = 2$, we have from these relations $f_{2c} \sin 2\theta = f_{2s} \cos 2\theta$, which is equivalent to the hydrodynamic condition $\Pi_{r\theta}|_{r=R} = 0$. For the third harmonic, the relations in Eq. (D2) yield $f_{3c} \cos 3\theta + f_{3s} \sin 3\theta = 0$, whence considering the first of Eq. (50), we obtain

$$\left(-\frac{\partial f_{2c}}{\partial x} + \frac{\partial f_{2s}}{\partial y} + \beta_3 \frac{\partial f_{2c}}{\partial y} + \beta_3 \frac{\partial f_{2s}}{\partial x}\right)_{r=R} \cos 3\theta - \left(\frac{\partial f_{2s}}{\partial x} + \frac{\partial f_{2c}}{\partial y} + \beta_3 \frac{\partial f_{2c}}{\partial x} - \beta_3 \frac{\partial f_{2s}}{\partial y}\right)_{r=R} \sin 3\theta = 0,$$

or equivalently

$$\left(-\frac{\partial \Pi_{xx}}{\partial x} + \frac{\partial \Pi_{xy}}{\partial y} + \beta_3 \frac{\partial \Pi_{xx}}{\partial y} + \beta_3 \frac{\partial \Pi_{xy}}{\partial x}\right)_{r=R} \cos 3\theta - \left(\frac{\partial \Pi_{xy}}{\partial x} + \frac{\partial \Pi_{xx}}{\partial y} + \beta_3 \frac{\partial \Pi_{xx}}{\partial x} - \beta_3 \frac{\partial \Pi_{xy}}{\partial y}\right)_{r=R} \sin 3\theta = 0.$$

From these equations rewritten in the polar coordinates, using the formulas:

$$\begin{aligned} \Pi_{rr} &= \Pi_{xx} \cos 2\theta + \Pi_{xy} \sin 2\theta, & \Pi_{r\theta} &= -\Pi_{xx} \sin 2\theta + \Pi_{xy} \cos 2\theta, \\ \Pi_{xy} &= \Pi_{rr} \sin 2\theta + \Pi_{r\theta} \cos 2\theta, & \Pi_{xx} &= \Pi_{rr} \cos 2\theta - \Pi_{r\theta} \sin 2\theta, \end{aligned} \quad (\text{F3})$$

we obtain the second condition in Eq. (58).

We emphasize that the first condition in Eq. (58) is exact, while the second condition is approximate since, in its derivation, the contribution of the fourth harmonic has been omitted in the expressions in Eq. (C1) for f_{3c} and f_{3s} .

APPENDIX G: CALCULATION OF TENSOR $\Pi_{\alpha\beta}$ IN THREE-HARMONIC APPROXIMATION

In this section, we construct the solution of the hydrodynamiclike equations for flow function $\psi(\mathbf{r}) = 2\text{Re}[\chi(r)e^{i\theta}]$, the electrostatic potential $\Phi(\mathbf{r}) = 2\text{Re}[f(r)e^{i\theta}]$, and the momentum flux $\Pi_{ik}(\mathbf{r}) = 2\text{Re}[Q_{ik}(r)e^{i\theta}]$ within the three-harmonic approximation. The differential operator on the left-hand side of the first in Eq. (67b) is zeroed by the two functions $1/r$ and $1/r^3$. Thus, we seek a solution in the form:

$$Q_{r\theta} = \frac{a}{r} + \frac{g(r)}{r^3},$$

where a is a constant, and $g(r)$ is a new unknown function. The equation for g is

$$\frac{\partial^2 g}{\partial r^2} - \frac{1}{r} \frac{\partial g}{\partial r} = r \frac{\partial F}{\partial r}.$$

It contains only derivatives of $g(r)$ and is easily solved. As a result, we have

$$\begin{aligned} Q_{r\theta} &= \frac{b}{r} + \frac{c}{r^3} + \frac{1}{r^3} \int rF(r)dr = \frac{b}{r} + \frac{c}{r^3} + \frac{1}{r^3} \int \left[2ir^2\varphi - \frac{m}{\tau} r^2 \frac{\partial(r\chi)}{\partial r} \right] dr \\ &= \frac{b}{r} + \frac{c}{r^3} - \frac{m}{\tau} \chi + \frac{2}{r^3} \int r^2 \left(i\varphi + \frac{m\chi}{\tau} \right) dr. \end{aligned}$$

Substituting here the expressions in Eqs. (62) and (63) and considering that $\int x^2 K_1(x)dx = -x^2 K_2(x)$, we obtain for the tensor $Q_{\alpha\beta}$:

$$\begin{aligned} Q_{r\theta} &= \frac{b}{r} + \frac{c}{r^3} + \frac{ir}{2} \left(\tilde{\alpha} + \frac{im}{\tau} \alpha \right) + \frac{i\tilde{\delta}}{r} - \frac{m}{\tau} [\gamma_+ K_1(\sqrt{\kappa_+}r) + \gamma_- K_1(\sqrt{\kappa_-}r)] \\ &\quad - \frac{2}{r} \left[\frac{1}{\sqrt{\kappa_+}} \left(i\tilde{\gamma}_+ + \frac{m}{\tau} \gamma_+ \right) K_2(\sqrt{\kappa_+}r) + \frac{1}{\sqrt{\kappa_-}} \left(i\tilde{\gamma}_- + \frac{m}{\tau} \gamma_- \right) K_2(\sqrt{\kappa_-}r) \right], \\ Q_{rr} &= -\frac{ib}{r} + \frac{ic}{r^3} + \varphi + \frac{2i}{r^3} \int r^2 \left(i\varphi + \frac{m\chi}{\tau} \right) dr \\ &= -\frac{ib}{r} + \frac{ic}{r^3} + \frac{ir}{2} \left(\tilde{\alpha} + \frac{im}{\tau} \alpha \right) + \frac{im\delta}{\tau r} + \tilde{\gamma}_+ K_1(\sqrt{\kappa_+}r) + \tilde{\gamma}_- K_1(\sqrt{\kappa_-}r) \\ &\quad - \frac{2i}{r} \left[\frac{1}{\sqrt{\kappa_+}} \left(i\tilde{\gamma}_+ + \frac{m}{\tau} \gamma_+ \right) K_2(\sqrt{\kappa_+}r) + \frac{1}{\sqrt{\kappa_-}} \left(i\tilde{\gamma}_- + \frac{m}{\tau} \gamma_- \right) K_2(\sqrt{\kappa_-}r) \right]. \end{aligned} \quad (\text{G1})$$

The last two formulas in Eq. (50) in radial variables r and θ take the form:

$$\Pi_{r\theta} = -mv \left(\frac{1}{r} \frac{\partial V_r}{\partial \theta} + \frac{\partial V_\theta}{\partial r} - \frac{V_\theta}{r} \right) - mv\beta_2 \left(\frac{\partial V_r}{\partial r} - \frac{1}{r} \frac{\partial V_\theta}{\partial \theta} - \frac{V_r}{r} \right)$$

$$\begin{aligned}
& + \frac{\nu\tau_3}{1+\beta_3^2}(1-\beta_2\beta_3)\left(\Delta\Pi_{r\theta} - \frac{4\Pi_{r\theta}}{r^2} + \frac{4\partial\Pi_{rr}}{r^2\partial\theta}\right) + \frac{\nu\tau_3}{1+\beta_3^2}(\beta_2+\beta_3)\left(\Delta\Pi_{rr} - \frac{4\Pi_{rr}}{r^2} - \frac{4\partial\Pi_{r\theta}}{r^2\partial\theta}\right), \\
\Pi_{rr} = & -mv\left(\frac{\partial V_r}{\partial r} - \frac{1}{r}\frac{\partial V_\theta}{\partial\theta} - \frac{V_r}{r}\right) + mv\beta_2\left(\frac{1}{r}\frac{\partial V_r}{\partial\theta} + \frac{\partial V_\theta}{\partial r} - \frac{V_\theta}{r}\right) \\
& + \frac{\nu\tau_3}{1+\beta_3^2}(1-\beta_2\beta_3)\left(\Delta\Pi_{rr} - \frac{4\Pi_{rr}}{r^2} - \frac{4\partial\Pi_{r\theta}}{r^2\partial\theta}\right) - \frac{\nu\tau_3}{1+\beta_3^2}(\beta_2+\beta_3)\left(\Delta\Pi_{r\theta} - \frac{4\Pi_{r\theta}}{r^2} + \frac{4\partial\Pi_{rr}}{r^2\partial\theta}\right). \quad (G2)
\end{aligned}$$

From Eqs. (G1) and (G2), using the definitions $V_r = -\partial\psi/r\partial\theta$, $V_\theta = \partial\psi/\partial r$ and Eqs. (62) and (63), it can be seen that the tensor Π should not contain linear-in- r terms, whence it follows $\tilde{\alpha} = -im\alpha/\tau$. Moreover, we can also see that there are no terms proportional to r^{-1} , which gives the relation $b = m\delta/\tau$ and one more connection between the constants: $\tilde{\delta} = im\delta/\tau$. Finally, the terms proportional to r^{-3} enter only in the hydrodynamic part of the tensor and have the form $-4m\nu\delta(1+i\beta)/r^3$ in the case of $\Pi_{r\theta}$ and $-4m\nu\delta(i-\beta)/r^3$ in the case of Π_{rr} . Comparing these relations with Eq. (G1), we obtain $c = -4m\nu(1+i\beta_2)\delta$.

In this way, all constants of integration are expressed via four quantities α , δ , γ_+ , and γ_- , which can be found from the four boundary conditions: the three on the edges of the disk and the one at infinity $\rho \rightarrow \infty$. In the following calculations, it will be convenient to use the dimensionless radius $\rho = r/R$, denote αR by α , δ/R by δ , and introduce the parameters $\varepsilon_- = \sqrt{\kappa_-}R \ll 1$ and $\varepsilon_+ = \sqrt{\kappa_+}R$. The tensor $Q_{\alpha\beta}$ is written as follows:

$$\begin{aligned}
Q_{r\theta} = & -\frac{4m\nu\delta}{R^2\rho^3}(1+i\beta_2) - \frac{m}{\tau}[\gamma_+K_1(\varepsilon_+\rho) + \gamma_-K_1(\varepsilon_-\rho)] - 2\left[\frac{1}{\varepsilon_+}\left(i\tilde{\gamma}_+ + \frac{m}{\tau}\gamma_+\right)K_2(\varepsilon_+\rho) + \frac{1}{\varepsilon_-}\left(i\tilde{\gamma}_- + \frac{m}{\tau}\gamma_-\right)K_2(\varepsilon_-\rho)\right], \\
Q_{rr} = & -i\frac{4m\nu\delta}{R^2\rho^3}(1+i\beta_2) + \tilde{\gamma}_+K_1(\varepsilon_+\rho) + \tilde{\gamma}_-K_1(\varepsilon_-\rho) - 2i\left[\frac{1}{\varepsilon_+}\left(i\tilde{\gamma}_+ + \frac{m}{\tau}\gamma_+\right)K_2(\varepsilon_+\rho) + \frac{1}{\varepsilon_-}\left(i\tilde{\gamma}_- + \frac{m}{\tau}\gamma_-\right)K_2(\varepsilon_-\rho)\right]. \quad (G3)
\end{aligned}$$

The boundary condition $V_r(1) = 0$ is equivalent, as it was in hydrodynamics, to the condition $\chi(1) = 0$, so from Eq. (62), we have

$$\delta = -\alpha - \gamma_+K_1(\varepsilon_+) - \gamma_-K_1(\varepsilon_-). \quad (G4)$$

The conditions $V_x(\infty) = V_x$ and $V_y(\infty) = V_y$ yield

$$\alpha = \frac{RV_y}{2} + i\frac{RV_x}{2} \equiv \alpha_1 + i\alpha_2. \quad (G5)$$

Since at $B \rightarrow 0$ the values $\tilde{\gamma}_-$ and γ_+ turn to zero, it is reasonable to use the coefficients γ_- and $\tilde{\gamma}_+$. The condition $Q_{r\theta}(1) = 0$ gives

$$-\frac{4m\nu\delta}{R^2}(1+i\beta_2) - \frac{m}{\tau}[\gamma_+K_1(\varepsilon_+) + \gamma_-K_1(\varepsilon_-)] - 2\left[\frac{1}{\varepsilon_+}\left(i\tilde{\gamma}_+ + \frac{m}{\tau}\gamma_+\right)K_2(\varepsilon_+) + \frac{1}{\varepsilon_-}\left(i\tilde{\gamma}_- + \frac{m}{\tau}\gamma_-\right)K_2(\varepsilon_-)\right] = 0. \quad (G6)$$

Finally, it is necessary to satisfy the second boundary condition in Eq. (58), which for the first harmonic is written as

$$\left[-\frac{\partial Q_{rr}}{\partial\rho} + 2Q_{rr} + \beta_3\left(\frac{\partial Q_{r\theta}}{\partial\rho} + iQ_{rr}\right)\right]_{\rho=1} = 0,$$

or considering Eq. (67) and the condition $\chi(1) = 0$, in the form:

$$\left[2(2+i\beta_3)Q_{rr} - \frac{\partial\Phi}{\partial\rho} + i\beta_3\left(\Phi + i\frac{m}{\tau}\frac{\partial\chi}{\partial\rho}\right)\right]_{\rho=1} = 0. \quad (G7)$$

Thus, we have the following system of equations for finding the values γ_- and $\tilde{\gamma}_+$:

$$\begin{aligned}
-\frac{4m\nu\delta}{R^2}(1+i\beta_2) - \frac{m}{\tau}[\gamma_+K_1(\varepsilon_+) + \gamma_-K_1(\varepsilon_-)] - 2i\left[\frac{1}{\varepsilon_+}\left(\tilde{\gamma}_+ - i\frac{m}{\tau}\gamma_+\right)K_2(\varepsilon_+) + \frac{1}{\varepsilon_-}\left(\tilde{\gamma}_- - i\frac{m}{\tau}\gamma_-\right)K_2(\varepsilon_-)\right] = 0, \\
\left[2(2+i\beta_3)Q_{rr} - \frac{\partial\Phi}{\partial\rho} + i\beta_3\left(\Phi + i\frac{m}{\tau}\frac{\partial\chi}{\partial\rho}\right)\right]_{\rho=1} = 0, \quad (G8)
\end{aligned}$$

where

$$Q_{rr}(1) = -i\frac{4m\nu\delta}{R^2}(1+i\beta_2) + \tilde{\gamma}_+K_1(\varepsilon_+) + \tilde{\gamma}_-K_1(\varepsilon_-) + 2\left[\frac{1}{\varepsilon_+}\left(\tilde{\gamma}_+ - i\frac{m}{\tau}\gamma_+\right)K_2(\varepsilon_+) + \frac{1}{\varepsilon_-}\left(\tilde{\gamma}_- - i\frac{m}{\tau}\gamma_-\right)K_2(\varepsilon_-)\right],$$

$$\delta = -\alpha - \gamma_+K_1(\varepsilon_+) - \gamma_-K_1(\varepsilon_-), \quad \frac{\partial\chi}{\partial\rho} = 2\alpha - \gamma_+\varepsilon_+K_0(\varepsilon_+) - \gamma_-\varepsilon_-K_0(\varepsilon_-),$$

$$\Phi(1) = -2i\frac{m}{\tau}\alpha + \left(\tilde{\gamma}_+ - i\frac{m}{\tau}\gamma_+\right)K_1(\varepsilon_+) + \left(\tilde{\gamma}_- - i\frac{m}{\tau}\gamma_-\right)K_1(\varepsilon_-),$$

$$\begin{aligned} \frac{\partial \Phi(1)}{\partial \rho} &= -2i\frac{m}{\tau}\alpha - \left(\tilde{\gamma}_+ - i\frac{m}{\tau}\gamma_+\right)K_1(\varepsilon_+) - \left(\tilde{\gamma}_- - i\frac{m}{\tau}\gamma_-\right)K_1(\varepsilon_-) - \tilde{\gamma}_+\varepsilon_+K_0(\varepsilon_+) - \tilde{\gamma}_-\varepsilon_-K_0(\varepsilon_-), \\ \Phi(1) + i\frac{m}{\tau}\frac{\partial \chi(1)}{\partial \rho} &= \left(\tilde{\gamma}_+ - i\frac{m}{\tau}\gamma_+\right)K_1(\varepsilon_+) + \left(\tilde{\gamma}_- - i\frac{m}{\tau}\gamma_-\right)K_1(\varepsilon_-) - i\frac{m}{\tau}\gamma_+\varepsilon_+K_0(\varepsilon_+) - i\frac{m}{\tau}\gamma_-\varepsilon_-K_0(\varepsilon_-). \end{aligned} \quad (\text{G9})$$

The formulas in Eq. (G9) have been derived using the identities $xK'_1(x) + K_1(x) = -xK_0(x)$ and $xK_2(x) = 2K_1(x) + xK_0(x)$. In this way, we have derived a close system of equations for the six constants α , δ , γ_{\pm} , and $\tilde{\gamma}_{\pm}$.

-
- [1] R. N. Gurzhi, Hydrodynamic effects in solids at low temperature, *Sov. Phys. Usp.* **11**, 255 (1968).
- [2] D. A. Bandurin, I. Torre, R. K. Kumar, M. Ben Shalom, A. Tomadin, A. Principi, G. H. Auton, E. Khestanova, K. S. Novoselov, I. V. Grigorieva *et al.*, Negative local resistance caused by viscous electron backflow in graphene, *Science* **351**, 1055 (2016).
- [3] L. Levitov and G. Falkovich, Electron viscosity, current vortices and negative nonlocal resistance in grapheme, *Nat. Phys.* **12**, 672 (2016).
- [4] A. I. Berdyugin, S. G. Xu, F. M. D. Pellegrino, R. K. Kumar, A. Principi, I. Torre, M. Ben Shalom, T. Taniguchi, K. Watanabe, I. V. Grigorieva *et al.*, Measuring Hall viscosity of graphene's electron fluid, *Science* **364**, 162 (2019).
- [5] J. A. Sulpizio, L. Ella, A. Rozen, J. Birkbeck, D. J. Perello, D. Dutta, M. Ben-Shalom, T. Taniguchi, K. Watanabe, T. Holder *et al.*, Visualizing Poiseuille flow of hydrodynamic electrons, *Nature (London)* **576**, 75 (2019).
- [6] M. J. H. Ku, T. X. Zhou, Q. Li, Y. J. Shin, J. K. Shi, C. Burch, L. E. Anderson, A. T. Pierce, Y. Xie, A. Hamo *et al.*, Imaging viscous flow of the Dirac fluid in graphene, *Nature (London)* **583**, 537 (2020).
- [7] P. J. W. Moll, P. Kushwaha, N. Nandi, B. Schmidt, and A. P. Mackenzie, Evidence for hydrodynamic electron flow in PdCoO₂, *Science* **351**, 1061 (2016).
- [8] J. Gooth, F. Menges, C. Shekhar, V. Suess, N. Kumar, Y. Sun, U. Drechsler, R. Zierold, C. Felser, and B. Gotsmann, Thermal and electrical signatures of a hydrodynamic electron fluid in tungsten diphosphide, *Nat. Commun.* **9**, 4093 (2018).
- [9] L. Bockhorn, P. Barthold, D. Schuh, W. Wegscheider, and R. J. Haug, Magnetoresistance in a high-mobility two-dimensional electron gas, *Phys. Rev. B* **83**, 113301 (2011).
- [10] A. T. Hatke, M. A. Zudov, J. L. Reno, L. N. Pfeiffer, and K. W. West, Giant negative magnetoresistance in high-mobility two-dimensional electron systems, *Phys. Rev. B* **85**, 081304(R) (2012).
- [11] R. G. Mani, A. Kriisa, and W. Wegscheider, Size-dependent giant-magnetoresistance in millimeter scale GaAs/AlGaAs 2D electron devices, *Sci. Rep.* **3**, 2747 (2013).
- [12] Q. Shi, P. D. Martin, Q. A. Ebner, M. A. Zudov, L. N. Pfeiffer, and K. W. West, Colossal negative magnetoresistance in a two-dimensional electron gas, *Phys. Rev. B* **89**, 201301(R) (2014).
- [13] L. Bockhorn, I. V. Gornyi, D. Schuh, C. Reichl, W. Wegscheider, and R. J. Haug, Magnetoresistance induced by rare strong scatterers in a high-mobility two-dimensional electron gas, *Phys. Rev. B* **90**, 165434 (2014).
- [14] G. M. Gusev, A. D. Levin, E. V. Levinson, and A. K. Bakarov, Viscous electron flow in mesoscopic two-dimensional electron gas, *AIP Adv.* **8**, 025318 (2018).
- [15] A. D. Levin, G. M. Gusev, E. V. Levinson, Z. D. Kvon, and A. K. Bakarov, Vorticity-induced negative nonlocal resistance in a viscous two-dimensional electron system, *Phys. Rev. B* **97**, 245308 (2018).
- [16] G. M. Gusev, A. D. Levin, E. V. Levinson, and A. K. Bakarov, Viscous transport and Hall viscosity in a two-dimensional electron system, *Phys. Rev. B* **98**, 161303(R) (2018).
- [17] P. S. Alekseev, Negative magnetoresistance in viscous flow of two-dimensional electrons, *Phys. Rev. Lett.* **117**, 166601 (2016).
- [18] Y. Dai, R. R. Du, L. N. Pfeiffer, and K. W. West, Observation of a cyclotron harmonic spike in microwave-induced resistances in ultraclean GaAs/AlGaAs quantum wells, *Phys. Rev. Lett.* **105**, 246802 (2010).
- [19] A. T. Hatke, M. A. Zudov, L. N. Pfeiffer, and K. W. West, Giant microwave photoresistivity in high-mobility quantum Hall systems, *Phys. Rev. B* **83**, 121301(R) (2011).
- [20] M. Bialek, J. Lusakowski, M. Czapkiewicz, J. Wrobel, and V. Umansky, Photoresponse of a two-dimensional electron gas at the second harmonic of the cyclotron resonance, *Phys. Rev. B* **91**, 045437 (2015).
- [21] P. S. Alekseev and A. P. Alekseeva, Transverse magnetosonic waves and viscoelastic resonance in a two-dimensional highly viscous electron fluid, *Phys. Rev. Lett.* **123**, 236801 (2019).
- [22] A. C. Keser, D. Q. Wang, O. Klochan, D. Y. H. Ho, O. A. Tkachenko, V. A. Tkachenko, D. Culcer, S. Adam, I. Farrer, D. A. Ritchie *et al.*, Geometric control of universal hydrodynamic flow in a two-dimensional electron fluid, *Phys. Rev. X* **11**, 031030 (2021).
- [23] A. Gupta, J. J. Heremans, G. Kataria, M. Chandra, S. Fallahi, G. C. Gardner, and M. J. Manfra, Hydrodynamic and ballistic transport over large length scales in GaAs/AlGaAs, *Phys. Rev. Lett.* **126**, 076803 (2021).
- [24] X. Wang, P. Jia, R.-R. Du, L. N. Pfeiffer, K. W. Baldwin, and K. W. West, Hydrodynamic charge transport in an GaAs/AlGaAs ultrahigh-mobility two-dimensional electron gas, *Phys. Rev. B* **106**, L241302 (2022).
- [25] G. M. Gusev, A. S. Jaroshevich, A. D. Levin, Z. D. Kvon, and A. K. Bakarov, Stokes flow around an obstacle in viscous two-dimensional electron liquid, *Sci. Rep.* **10**, 7860 (2020).
- [26] A. Lucas, Stokes paradox in electronic Fermi liquids, *Phys. Rev. B* **95**, 115425 (2017).
- [27] B. Horn-Cosfeld, J. Schluck, J. Lammert, M. Cerchez, T. Heinzl, K. Pierz, H. W. Schumacher, and D. Mailly, Rel-

- evance of weak and strong classical scattering for the giant negative magnetoresistance in two-dimensional electron gases, *Phys. Rev. B* **104**, 045306 (2021).
- [28] M. Hruska and B. Spivak, Conductivity of the classical two-dimensional electron gas, *Phys. Rev. B* **65**, 033315 (2002).
- [29] H. Guo, E. Ilseven, G. Falkovich, and L. Levitov, Higher-than-ballistic conduction of viscous electron flows, *Proc. Natl Acad. Sci. USA* **114**, 3068 (2017).
- [30] J. Kozeny, Über kapillare Leitung des Wassers im Boden, Sitz.-Ber K. Akad. Wiss. **136(2a)**, 271 (1927).
- [31] P. C. Carman, Fluid flow through granular beds, *Chem. Eng. Res. Des.* **75**, S32 (1997).
- [32] H. C. Brinkman, A calculation of the viscous force exerted by a flowing fluid on a dense swarm of particles, *Appl. Sci. Res.* **A1**, 27 (1949).
- [33] S. Childress, Viscous flow past a random array of spheres, *J. Chem. Phys.* **56**, 2527 (1972).
- [34] J. Rubinstein, On the macroscopic description of slow viscous flow past a random array of spheres, *J. Stat. Phys.* **44**, 849 (1986).
- [35] S. Kuwabara, The forces experienced by randomly distributed parallel circular cylinders or spheres in a viscous flow at small Reynolds numbers, *J. Phys. Soc. Jap.* **14**, 527 (1959).
- [36] J. Happel, Viscous flow in multiparticle systems: Slow motion of fluids relative to beds of spherical particles, *AIChE J.* **4**, 197 (1958).
- [37] J. Happel, Viscous flow relative to arrays of cylinders, *AIChE J.* **5**, 174 (1959).
- [38] G. H. Neale and W. K. Nader, Prediction of transport processes within porous media: Creeping flow relative to a fixed swarm of spherical particles, *AIChE J.* **20**, 530 (1974).
- [39] T. S. Lundgren, Slow flow through stationary random beds and suspensions of spheres, *J. Fluid Mech.* **51**, 273 (1972).
- [40] C. K. W. Tam, The drag on a cloud of spherical particles in low Reynolds number flow, *J. Fluid Mech.* **38**, 537 (1969).
- [41] T. Scaffidi, N. Nandi, B. Schmidt, A. P. Mackenzie, and J. E. Moore, Hydrodynamic electron flow and Hall viscosity, *Phys. Rev. Lett.* **118**, 226601 (2017).
- [42] T. Holder, R. Queiroz, T. Scaffidi, N. Silberstein, A. Rozen, J. A. Sulpizio, L. Ella, S. Ilani, and A. Stern, Ballistic and hydrodynamic magnetotransport in narrow channels, *Phys. Rev. B* **100**, 245305 (2019).
- [43] P. S. Alekseev and M. A. Semina, Hall effect in a ballistic flow of two-dimensional interacting particles, *Phys. Rev. B* **100**, 125419 (2019).
- [44] Yu. O. Alekseev and A. P. Dmitriev, Giant Hall effect in the ballistic transport of two-dimensional electrons, *Phys. Rev. B* **104**, 085434 (2021).
- [45] A. N. Afanasiev, P. S. Alekseev, A. A. Greshnov, and M. A. Semina, Ballistic-hydrodynamic phase transition in flow of two-dimensional electrons, *Phys. Rev. B* **104**, 195415 (2021).
- [46] A. N. Afanasiev, P. S. Alekseev, A. A. Danilenko, A. P. Dmitriev, A. A. Greshnov, and M. A. Semina, Hall effect in Poiseuille flow of two-dimensional electron fluid, *Phys. Rev. B* **106**, 245415 (2022).
- [47] E. I. Kiselev and J. Schmalian, Boundary conditions of viscous electron flow, *Phys. Rev. B* **99**, 035430 (2019).
- [48] O. E. Raichev, Linking boundary conditions for kinetic and hydrodynamic description of fermion gas, *Phys. Rev. B* **105**, L041301 (2022).
- [49] C. Herring, Effect of random inhomogeneities on electrical and galvanomagnetic measurements, *J. Appl. Phys.* **31**, 1939 (1960).
- [50] P. S. Alekseev and A. P. Dmitriev, Viscosity of two-dimensional electrons, *Phys. Rev. B* **102**, 241409(R) (2020).
- [51] Y. M. Beltukov and M. I. Dyakonov, Microwave-induced resistance oscillations as a classical memory effect, *Phys. Rev. Lett.* **116**, 176801 (2016).
- [52] P. S. Alekseev and A. P. Alekseeva, Highly correlated two-dimensional electron fluid in moderate magnetic fields, [arXiv:2105.01035](https://arxiv.org/abs/2105.01035).
- [53] S. V. Gantsevich, V. L. Gurevich, and R. Katilius, Theory of fluctuations in nonequilibrium electron gas, *Riv. Nuovo Cim.* **2**, 1 (1979).
- [54] V. D. Kagan, Fluctuation in a system of charged particles, *Sov. Phys. Solid State* **17**, 1289 (1975).